

# Changes in electric-field noise due to thermal transformation of a surface ion trap

Maya Berlin-Udi,<sup>1,2</sup> Clemens Matthiesen,<sup>1</sup> P. N. Thomas Lloyd,<sup>1,\*</sup> Alberto Alonso,<sup>1,2</sup> Crystal Noel,<sup>1,†</sup> Chris Orme,<sup>3</sup> Chang-Eun Kim,<sup>3</sup> Vincenzo Lordi,<sup>3</sup> and Hartmut Häffner<sup>1,2</sup>

<sup>1</sup>*Department of Physics, University of California, Berkeley, California 94720, USA*

<sup>2</sup>*Challenge Institute for Quantum Computation, University of California, Berkeley, CA 94720*

<sup>3</sup>*Lawrence Livermore National Laboratory, Livermore, CA, 94551, USA*

(Dated: December 23, 2024)

We aim to illuminate how the microscopic properties of a metal surface map to its electric-field noise characteristics. In our system, prolonged heat treatments of a metal film can induce a rise in the magnitude of the electric-field noise generated by the surface of that film. We refer to this heat-induced rise in noise magnitude as a thermal transformation. The underlying physics of this thermal transformation process is explored through a series of heating, milling, and electron treatments performed on a single surface ion trap. Between these treatments,  $^{40}\text{Ca}^+$  ions trapped 70  $\mu\text{m}$  above the surface of the metal are used as detectors to monitor the electric-field noise at frequencies close to 1 MHz. An Auger spectrometer is used to track changes in the composition of the contaminated metal surface. With these tools we investigate contaminant deposition, chemical reactions, and atomic restructuring as possible drivers of thermal transformations. The data suggest that the observed thermal transformations can be explained by atomic restructuring at the trap surface. We hypothesize that a rise in local atomic order increases surface electric-field noise in this system.

## I. INTRODUCTION

Surface electric-field noise describes the fluctuation of an electric field due to charge movement in the surface of a material. Noise from metal surfaces is of particular interest to the ion trapping community, as metal electrodes, necessary to define the electric fields in an ion trap, constitute the nearest surfaces to the ions. Such ions are trapped in harmonic potentials, and electric-field noise resonant with the motional modes of the trap can cause ion heating and motional decoherence. These processes are detrimental to applications of trapped ions including quantum information processing and tests of fundamental physics [1, 2].

While it is generally understood that dynamic processes such as defect hopping and contaminant diffusion take place at metal surfaces, it is not known which microscopic processes specifically dominate charge dynamics and lead to surface electric-field noise. Advancing our understanding of surface charge dynamics could open new avenues for ion trap engineering. It could also benefit other technologies which suffer from charge noise or surface noise of various kinds, both within the field of quantum information processing, and beyond. This includes solid-state qubits in diamond [3, 4], superconducting qubits [5, 6], single-electron transistors [7], Casimir force detection [8], and precise measurements of gravitational fields [9, 10].

Measurements of electric-field noise in ion traps have yielded a wide variety of results between different research groups and different traps across a range of studied parameters, such as the noise magnitudes, frequency and distance dependencies, and the response to surface treatments [1]. Such variations indicate that no single physical process is responsible for all surface noise. Most likely, in any given system there are multiple competing mechanisms at play [11]. To gain a general understanding of electric-field noise from metal surfaces, we must first disentangle these mechanisms through in-depth studies of individual surfaces.

Several different types of surface treatments have been performed on ion traps in various efforts to understand and reduce noise. Laser ablation reduced electric-field noise by about 50% in one ion trap [12]. Ion milling reduced noise by up to two orders of magnitude in several investigations [11, 13–15], and oxygen plasma reduced noise by a factor of four according to one report [16]. In all cases, these treatments removed contamination from the surface of the trap electrodes. These results suggest that surface contaminants may play an important role in generating electric-field noise in ion traps.

However, the relationship between contamination and electric-field noise is not straightforward. Daniilidis *et al.* [13] found that a trap recontaminated after milling still maintained a low noise magnitude. Sedlacek *et al.* [11] observed that for some materials, ion milling actually increased noise at cryogenic temperatures, and Kim *et al.* [17] found that noise first rose and then fell in response to a series of small-dose ion milling treatments.

Given that noise magnitudes have not been found to be directly proportional to contaminant levels on ion trap surfaces, it is likely that contaminant removal is not solely responsible for the observed treatment-induced noise reductions. Here we aim to determine how ion milling and

---

\* Current address: Department of Physics, University of Santa Barbara, Santa Barbara, California 93106, USA

† Current address: Joint Quantum Institute, Center for Quantum Information and Computer Science, and Departments of Physics and Electrical and Computer Engineering, University of Maryland, College Park, MD 20742, USA

other surface treatments can affect surface noise levels at a microscopic level. By understanding the mechanisms behind noise reduction and promotion, we can determine which surface properties correspond to high and low noise levels. We anticipate that this information will help in the design of low-noise quantum devices.

We use trapped  $^{40}\text{Ca}^+$  ions as detectors to study the noise generated by the surface of an aluminum-copper ion trap. We measure noise at multiple temperatures and frequencies, and then observe how the noise responds to changes in the properties of the trap surface. The surface properties are altered using treatments including prolonged heating, argon ion milling, and electron bombardment. The trap surface composition is tracked via *in situ* Auger spectroscopy. The measured noise characteristics for our trap are consistent with noise produced by an ensemble of thermally activated fluctuators [18], so our data are discussed in this context.

We have observed that argon ion milling reduces noise at frequencies near 1-MHz, while altering the composition of the trap surface. We have further observed that prolonged heat treatments can increase the room-temperature noise magnitude without altering the surface composition. The latter provides us with an opportunity to study how noise is correlated to a surface property other than the contaminant level or temperature, which have both been previously studied.

In this manuscript, we will explore the underlying physics of the thermal transformations observed in our system. A thermal transformation is a sustained change in the noise spectrum (over a defined temperature and frequency range), caused by the thermally driven modification of the physical properties of the noise source. Such modifications may include processes such as the addition, removal, or restructuring of material. A thermal transformation is distinct from a thermal noise activation. When noise is thermally activated, the noise spectrum changes in a predictable and reversible fashion determined by the characteristic activation energy. Thermally activated noise thus has a repeatable temperature dependence, and might stem from noise sources such as thermally activated fluctuators [18] or fluctuating dipoles [19]. In contrast, noise that is being thermally transformed does not have a repeatable temperature dependence, i.e. the characteristics of the noise source are permanently altered by the thermal process.

The manuscript is organized as follows. In Sec. II, we discuss the methods we use to treat and characterize the ion trap surface. In Sec. III we present results from a wide range of measurements taken throughout our study of thermal noise transformations. These include measurements of ion heating rates as a function of temperature, which can be directly translated to an electric-field noise temperature scaling. Additional measurements include Auger spectra, which provide information on the atomic and chemical composition of the surface, and *ex situ* AFM data which can be used to characterize the surface morphology. We also report how

ion heating rates change in response to heat treatments, electron bombardment, and argon ion milling. In Sec. IV we analyze and interpret our measurement results, and explore contaminant deposition, chemical reactions and atomic restructuring as possible drivers of thermal noise transformations. Finally, in Sec. V we speculate that thermal transformations correspond to a increase in local atomic order, and discuss mechanisms through which this phenomenon could cause a rise in surface electric-field noise.

## II. METHODS

We perform a series of *in situ* surface treatments on a single rf quadrupole surface ion trap without breaking vacuum. The base pressure of the vacuum chamber is about  $1 \times 10^{-10}$  Torr. The surface trap under investigation is composed of an insulating fused silica substrate and a conductive metal surface. Trenches are etched into the fused silica to define (and provide electrical isolation between) rf and dc electrodes. These electrodes are biased or driven in order to generate the confining electric fields necessary for trapping ions.

Six layers of metal were deposited onto the trap surface via electron-beam evaporation. The first layer is 15 nm thick and composed of titanium to act as a sticking agent, followed by 500 nm of aluminum and 30 nm of copper. After these three layers were deposited, the trap was briefly exposed to atmosphere as the trap was rotated, and then an additional 15 nm of titanium, 500 nm of aluminum and 30 nm of copper were deposited. Subsequent heating in the experiment vacuum chamber caused the metal layers to intermix. The trap was stored in atmosphere both before and after baking for a cumulative exposure time of 30 weeks, causing the trap surface to oxidize and accumulate contaminants such as organic adsorbates.

This trap is designed to hold ions in a harmonic potential 70  $\mu\text{m}$  above the metal surface. The motional modes of a trapped ion have well-defined frequencies in the MHz range. When exposed to electric-field noise at these frequencies, the ion motion heats up. Measuring the heating rate of the motion allows us to use the ion as an ultra-sensitive narrow-band electric-field noise detector. We measure the motional heating rate of a single trapped  $^{40}\text{Ca}^+$  ion by tracking the decay of carrier Rabi oscillations [20]. The electric-field noise power spectral density  $S_E(\omega)$  is directly proportional to the ion motional heating rate  $\dot{n}$  according to [1]:

$$S_E(\omega) = \frac{4m\hbar\omega}{q^2} \dot{n}(\omega), \quad (1)$$

where  $m$  and  $q$  are the mass and the charge of the ion,  $\hbar$  is the reduced Planck constant, and  $\omega$  is the secular trap frequency.  $S_E(\omega)$  is a measure of the amplitude of the electric-field noise at frequency  $\omega$ .

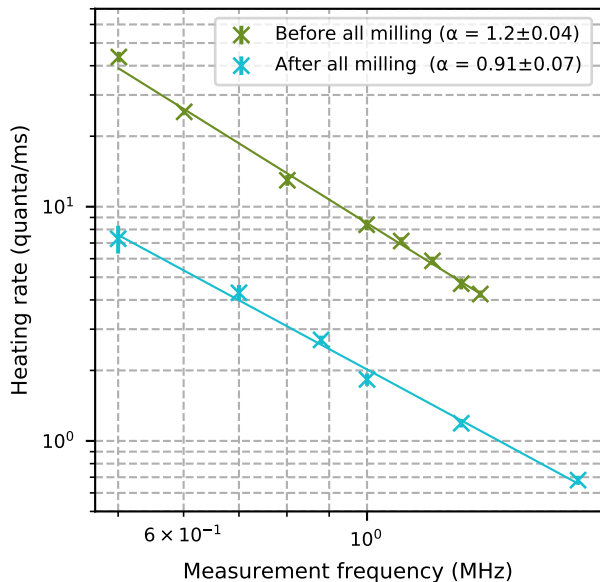


FIG. 1: Ion heating rates measured as a function of frequency at room temperature. The heating rate scales inversely with frequency. The frequency scaling exponent  $\alpha$  is close to one, both before and after surface treatment.

By altering the ion confinement potential, we can measure noise at frequencies anywhere between  $2\pi \times 0.5$  MHz and  $2\pi \times 2$  MHz. Two sets of measurements are shown in Fig. 1. We find that the ion heating rates follow a power-law dependence as

$$\dot{n} \propto 1/f^{\alpha+1}, \quad (2)$$

where  $f$  is the noise frequency and  $\alpha$  is the frequency scaling exponent. According to Eq. (1), the surface electric-field noise in our system then scales as  $1/f^\alpha$ . We measured  $\alpha$  to be close to 1 both before and after surface treatments. This suggests that these surface treatments may not fundamentally change the nature of the dominant noise mechanisms.

The trap is clamped to a resistive button heater, which enables us to measure how the surface noise depends on the temperature of the ion trap chip. We monitor the trap temperature using a thermal imaging camera. This experimental setup is described in Ref. [18]. We are able to measure ion heating rates when the chip temperature is between room temperature and 600 K. At higher temperatures, the ion lifetime becomes too short to perform measurements.

Ion heating rates measured as a function of the temperature of our ion trap chip are plotted in Fig. 2. At approximately 575 K, heating rates begin to rise rapidly. This high-temperature behavior endured qualitatively throughout all surface treatments. This may be evidence that a new noise mechanism becomes dominant above 575 K in our trap. In this manuscript we will focus only

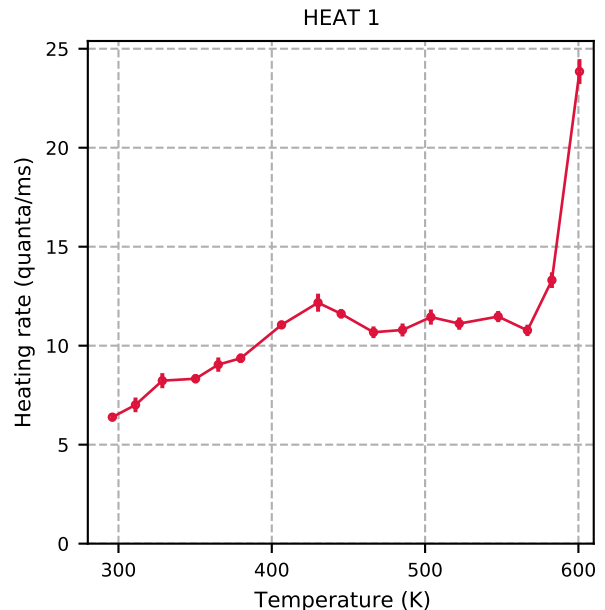


FIG. 2: Ion heating rates measured as a function of ion trap substrate temperature. Measurements were performed at trap frequency  $2\pi \times 1.3$  MHz.

on the mechanisms dominant at lower temperatures and report heating rates measured up to 550 K in the following [21].

We will focus on ten heat treatments that we performed on a single surface ion trap. A heat treatment involves the heating of the substrate to temperatures greater than 500 K for a period of days. The parameters of these heat treatments are summarized in Tab. I, and plotted in detail in App. B. Fig. 2 shows data recorded at the end of treatment HEAT 1. Each heat treatment was immediately preceded by argon ion milling, with the exception of HEAT 1, which was performed before any milling took place.

We performed Argon ion milling with ion energies between 200 and 500 eV. The argon pressure in the chamber during these treatments was approximately  $10^{-5}$  mbar, and ion currents ranged from 5 to 10  $\mu\text{A}/\text{cm}^2$ . The ion beam was angled normal to the trap surface during all treatments, except in the final milling step performed before HEAT 10, when the beam was at a  $45^\circ$  angle. Each milling treatment was performed for a different period of time. The details of each milling treatment can be found in App. B. We used the SRIM software [22] to determine the amount of material removed in each milling step, taking into account ion energy, ion current, milling duration, and surface composition as measured with Auger spectroscopy. The estimated cumulative material removed by the start of each heat treatment is shown in Tab. I. The cumulative milling energy for all argon ion treatments was  $42 \text{ J}/\text{cm}^2$ .

An Auger spectrometer is installed *in situ*, so that heat

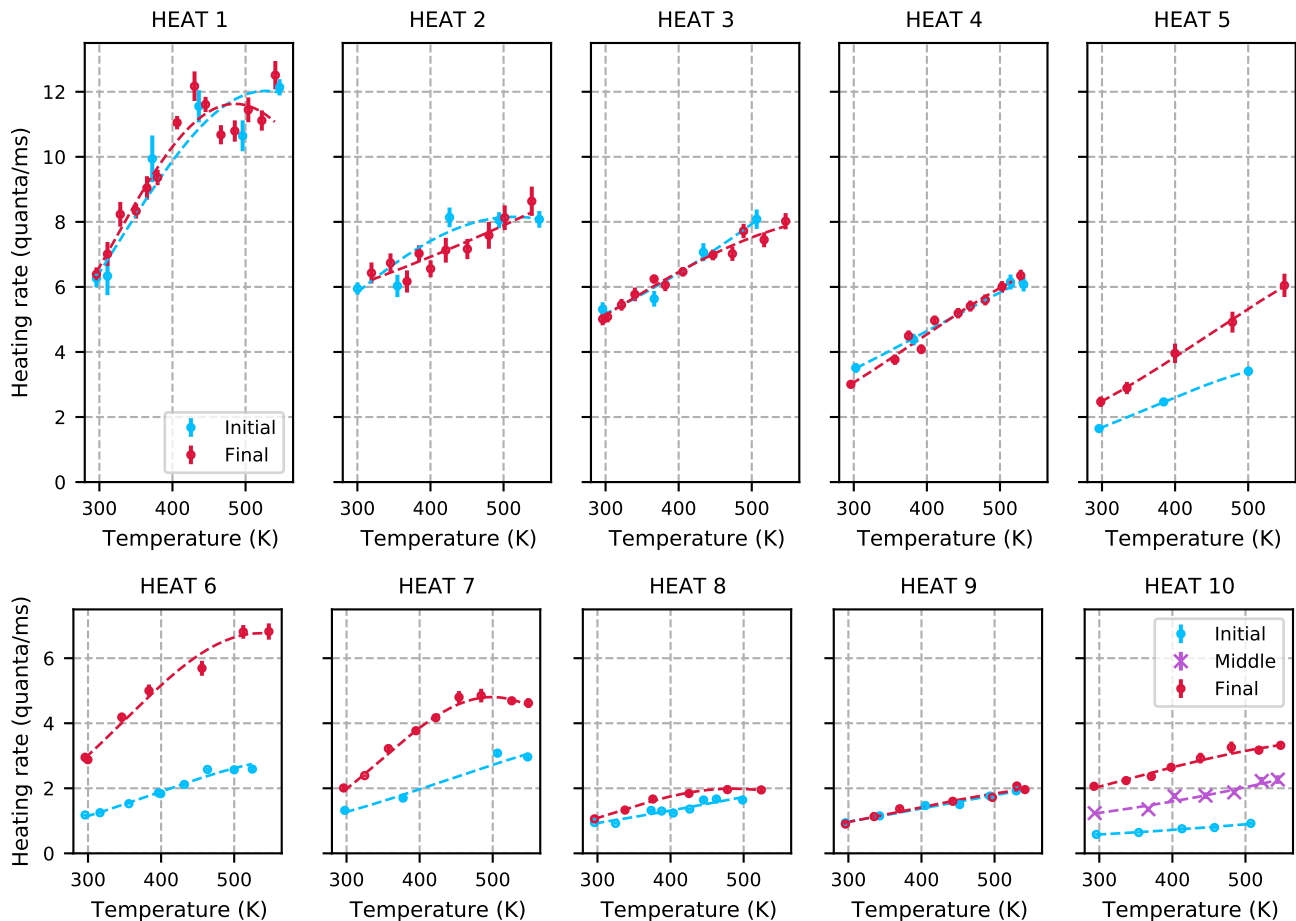


FIG. 3: Ion heating rates measured as a function of substrate temperature during ten heat treatments. The *initial* heating rates were measured as the temperature of the substrate was raised at the start of each treatment. The *final* heating rates were measured after the substrate was held at temperatures greater than 500 K for multiple days. Thermal transformations are observed in HEAT 5, 6, 7, 10 and to a lesser degree HEAT 8. The trap was milled with argon ions between heat treatments. Information on milling and heat treatment parameters can be found in App. B and in Tab. I. The HEAT 1, 3, 4, 6, 7, 8, and 9 measurements plotted here were performed at trap frequency  $2\pi \times 1.3$  MHz. The HEAT 2, 5, and 10 measurements plotted here were performed at trap frequency  $2\pi \times 0.88$  MHz and scaled to  $2\pi \times 1.3$  MHz assuming  $\alpha = 1$  for the purposes of this figure.

treatments, argon ion milling, ion heating rate measurements and surface composition measurements can all be performed without breaking vacuum. We use an OCI Vacuum Microengineering Inc. Auger spectrometer with a retarding field analyzer, and a lock-in amplifier that allows us to record the differential Auger spectrum. This method is sensitive to the top 3 to 10 monolayers of a substrate, depending on its material composition. To determine the fractional composition of the trap surface, we match the measured peaks to spectra of known elements, then measure the peak-to-peak magnitude for each element, and scale by a sensitivity factor provided by the manufacturer of the spectrometer.

Our Auger spectroscopy involves bombarding the trap surface with 2 keV electrons, and then measuring the amplitude of Auger electrons emitted from the trap surface. At the center of the electron beam, the current

density is between 3 and 12 mA/cm<sup>2</sup>. This incident electron beam can also be used as a surface treatment in its own right. When performing an electron treatment, the electron beam is aligned such that it bombards the trap surface directly below where the calcium ions can be trapped. When we want to measure the surface composition without altering the the surface at the trapping position, we record an Auger spectrum with the electron beam aligned away from this area.

### III. RESULTS

We measured the heating rate as a function of substrate temperature during ten heat treatment experiments. The measurement results are plotted in Fig. 3. The trap was milled with argon ions before each heat

TABLE I: Summary of the temperatures and timings of ten heat treatments performed on our ion trap. The *cumulative material removed* refers to estimates (see text) of the total thickness of material that was removed from the surface of the trap via argon ion milling between the trap’s fabrication and the start of each heat treatment. Additional details of the heat treatment procedures are plotted in App. B.

Treatment	Time over 550 K (days)	Time over 575 K (days)	Cumulative material removed (nm)	Most recent mill dose ( $\text{J}/\text{cm}^2$ )
HEAT 1	2.5	2	0	0
HEAT 2	3	3	0.13	0.1
HEAT 3	2	0.3	0.26	0.1
HEAT 4	1.5	1	0.86	0.5
HEAT 5	5	3	6.3	2.9
HEAT 6	4	0.2	17.7	7.5
HEAT 7	7	4	34	8.8
HEAT 8	4.5	3.5	36	0.6
HEAT 9	3	3	48	4.9
HEAT 10	20	9	77	5.2

treatment, and this milling caused ion heating rates to steadily decrease in magnitude. In some temperature-dependence measurements, the heating rate increased monotonically with temperature. In other experiments the temperature dependence saturated at high temperatures, or, in the case of HEAT 7 Final, decreased slightly at high temperatures.

In some of these experiments, the temperature dependence of the ion heating rate did not change as a result of the heat treatment. In other experiments, the substrate’s prolonged exposure to high temperatures caused thermal transformations to take place, and the ion heating rates increased across the measured temperature range. Thermal transformations took place during treatments HEAT 5, 6, 7, 10 and, to a lesser extent, HEAT 8. Details of the timings and temperatures of heat treatments are presented in App. B, and a summary can be found in Table I.

Following this overview of the heating rate data, we present results from a range of surface treatments with a focus on how they relate to the thermal transformation process.

*Thermal transformation dynamics:* To quantify the timescale of the thermal transformation process, we raised the substrate temperature relatively swiftly to 575 K at the start of HEAT 7, and repeatedly measured the ion heating rates at 575 K for a full week. Heating rates rose steadily for the first few days, and then the noise transformation saturated. The parameters of this heat treatment, and the corresponding ion-heating-rate measurement results, are presented in Fig. 4.

The constant-temperature heating rate measurements from HEAT 7, as plotted in Fig. 4, are fit to a simple exponential saturation function:

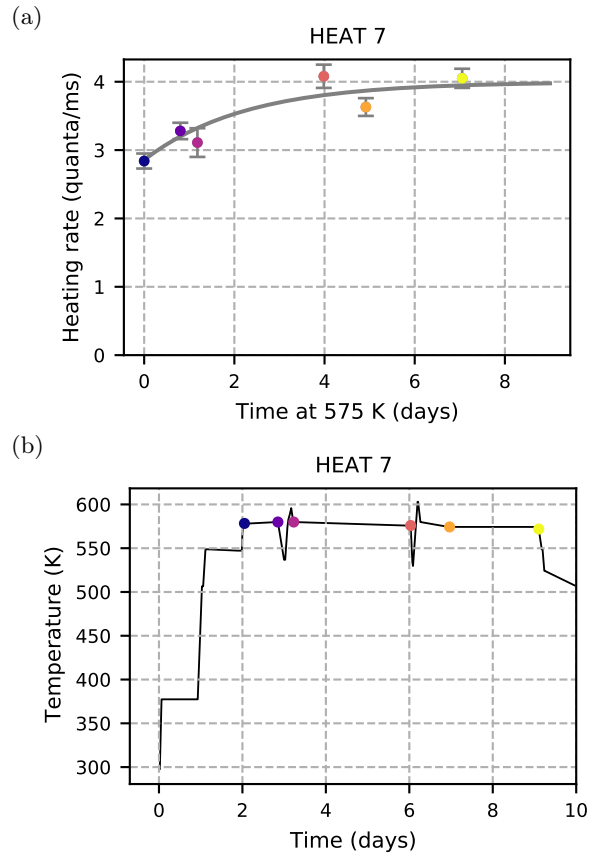


FIG. 4: Ion heating rates measured during treatment HEAT 7 while the substrate temperature was held at 575 K show a saturating noise transformation with a half life of  $1.6 \pm 0.8$  days. (a) The time dependence of ion heating rates, fit to Eq. 3. (b) Timing and temperatures of treatment HEAT 7. To determine the context in which each measurement was taken, match the colors of the data plotted in (a) to the colors of the data in (b). These heating rates were measured at  $2\pi \times 1.3$  MHz.

$$\Gamma = \Gamma_0 + A(1 - e^{-kt}) \quad (3)$$

where  $\Gamma$  is the ion heating rate at 575 K,  $t$  is the time spent at 575 K, and  $\Gamma_0$ , amplitude  $A$  and rate constant  $k$  are fit parameters. The half life  $\lambda$  of this transformation can be calculated directly from the rate constant  $k$  as  $\lambda = \ln(2)/k$ , yielding a half life of  $1.6 \pm 0.8$  days for the noise transformation at 575 K.

During treatment HEAT 10, the trap temperature was held between 555 and 580 K for twelve days, as shown in Fig. 5. During this time, we measured the ion heating rate repeatedly at 555 K. The heating rate initially appeared to saturate. However, after subsequent temperature cycling the heating rate had increased. Raising the trap temperature above 600 K for a period of 3.5 days, we found the ion heating rate rose by an additional 50%.

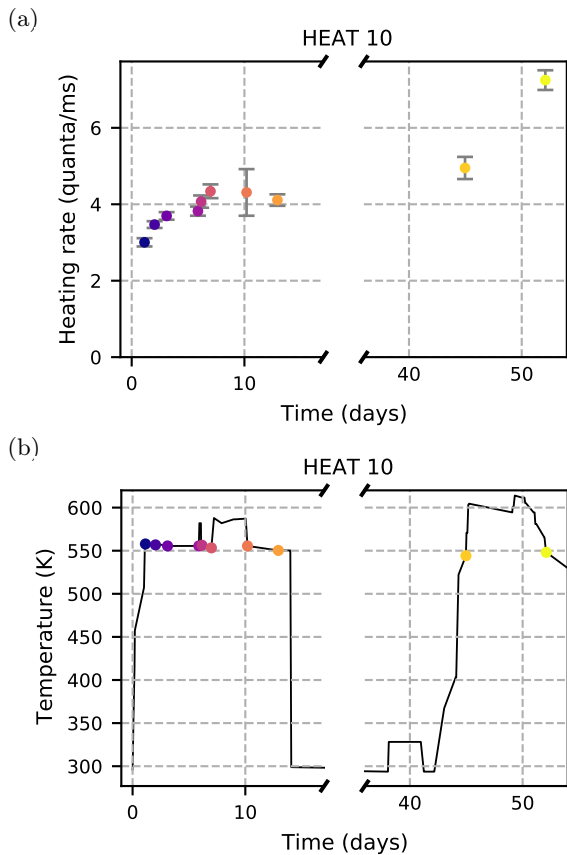


FIG. 5: Ion heating rates were repeatedly measured at 550 K during treatment HEAT 10. (a) The time dependence of ion heating rates. (b) Timing and temperatures of treatment HEAT 10. To determine the context in which each measurement was taken, match the colors of the data plotted in (a) to the colors of the data in (b). These heating rates were measured at  $2\pi \times 0.88$  MHz.

*Ion milling of thermally transformed surfaces:* The surface of the trap was milled with argon ions between each heat treatment. After HEAT 6, during which a significant thermal transformation took place, 16 nm of material was milled away from the trap surface. As shown in Fig. 6a, this milling treatment brought the ion heating rates down to pre-transformation levels.

We performed a series of small-dose milling treatments after the HEAT 7 thermal transformation, removing 0.6 nm and then 1.3 nm of material from the trap surface. The incident argon ions had an energy of 200 eV, and we estimate that they penetrated about 2 nm into the metal [22]. The temperature dependence of the ion heating rate was measured after each of these treatments. As shown in Fig. 6b, these small milling treatments had a significant impact on the ion heating rate. Although only a few nanometers of material was affected by milling, the heating rates were brought down nearly to pre-transformation levels.

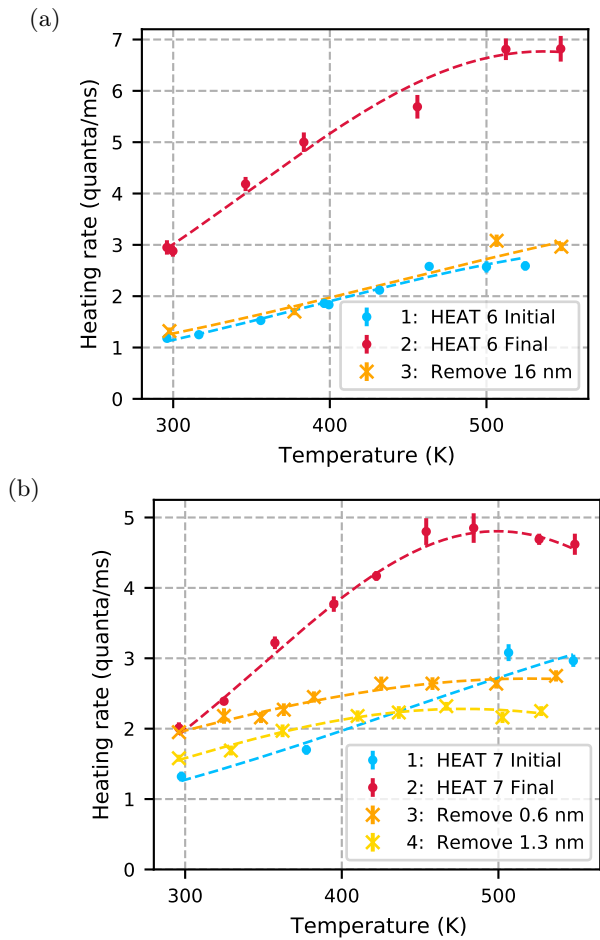


FIG. 6: (a) Treatment HEAT 6 drove a thermal transformation which raised the ion heating rates. The subsequent ion milling removed 16 nm of material and brought the heating rates back down. (b) Treatment HEAT 7 drove a thermal transformation which raised ion heating rates. The subsequent small milling doses removed a total of 2 nm of material, and brought the heating rates down nearly to pre-transformation levels. These heating rates were measured at  $2\pi \times 1.3$  MHz.

*Electron bombardment:* Electron treatments were performed on the trap surface immediately after HEAT 9, when the trap was heated but not transformed, and immediately after HEAT 10, when the trap underwent a thermal transformation. We measured the temperature dependence of the ion heating rates before and after these electron treatments, and the results are plotted in Fig. 7. The change in the heating-rate temperature dependence due to electron treatments was comparable in both cases, with ion heating rates slightly increasing at high temperatures as compared to the pre-electron-treatment measurements.

*Auger spectroscopy:* Auger spectra were measured at various times throughout our experiments in an effort to characterize the composition of the trap surface. Data from three of these measurements are plotted in Fig. 8.

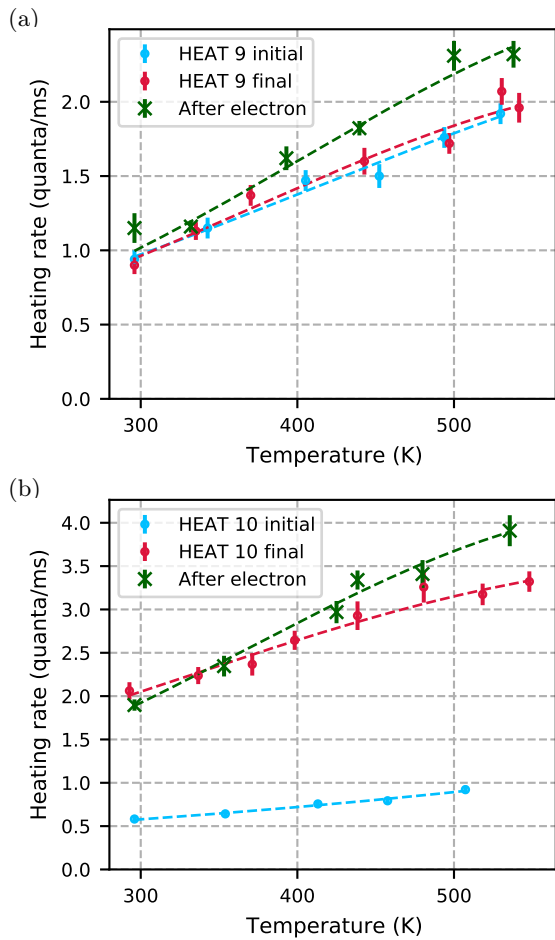


FIG. 7: Temperature dependence of ion heating rates measured before and after the trap surface was bombarded by a 2 keV electron beam for 3.2 hours. (a) Electron treatment of 180 kJ/cm<sup>2</sup> performed after HEAT 9, a heat treatment in which the noise did not thermally transform. These heating rates were measured at  $2\pi \times 1.3$  MHz. (b) Electron treatment of 280 kJ/cm<sup>2</sup> performed immediately after HEAT 10, when the noise underwent a significant thermal transformation. These heating rates were measured at  $2\pi \times 0.88$  MHz and scaled to a frequency of  $2\pi \times 1.3$  MHz assuming  $\alpha = 1$  for the purposes of this figure.

The peaks visible in these spectra indicate the presence of aluminum, copper, titanium, oxygen, carbon, nitrogen and argon. Comparing the spectra measured before and after the HEAT 7 thermal transformation (middle and bottom curves), we deduce that no significant quantities of new elements were introduced to the trap surface during the heat treatment. In addition, the relative peak heights of different elements are nearly identical before and after heating. This is the case for all spectra measured before and after heat treatments, as shown in App. A. In contrast, milling the surface had a significant impact on its composition (top and middle curves in Fig. 8).

Surface compositions corresponding to six of the ten heat treatments are shown in Fig. 9. The corresponding Auger measurements were performed immediately before treatments HEAT 1, HEAT 6, HEAT 7, HEAT 8 and HEAT 10, and immediately after HEAT 9. The Auger spectra from which these surface compositions were extracted can be found in App. A. The surface composition was not measured immediately before or after treatments HEAT 2, 3, 4 or 5.

In addition to containing information about the atomic composition of the trap, Auger spectra also allow us to determine the chemical state of the aluminum at the trap surface. The aluminum state can be deduced from the lineshape of the aluminum Auger peaks, combined with the ratio of aluminum to other elements. Aluminum Auger spectra taken before or after six of the ten heat treatments are shown in Fig. 10.

The ratio of oxygen to aluminum at the trap surface was greater than 1:1 during HEAT 1, as shown in Fig. 9. This, in combination with a shift of the 1404 eV Auger peak by -8 eV, as shown in Fig. 10, is indicative of oxidized aluminum [23]. This is consistent with the trap's history, as it had been exposed to atmosphere but not yet milled at the start of HEAT 1. Given the large carbon signal, there may also have been aluminum carbide present at this time.

The aluminum spectra measured before HEAT 6, 7, and 10, and plotted in Fig. 10, each have five distinct peaks and qualitatively match spectra of elemental aluminum [24] [25]. The corresponding surface compositions plotted in Fig. 9 show that the surface contamination was relatively low during these heat treatments, which is consistent with the aluminum being primarily elemental.

The aluminum spectra measured before HEAT 8 and after HEAT 9, are plotted in Fig. 10. The small negative energy shift of the primary peak 1404 eV, and the reduction of the satellite peaks at 1135, 1369 and 1387 eV, are indicative of aluminum nitride [23]. The corresponding surface fractions, shown in Fig. 9, show significant levels of both oxygen and nitrogen. We conclude that during these heat treatments, the aluminum surface was partially oxidized, and partially took the form of aluminum nitride. It is unclear whether the oxygen and nitrogen were embedded in the bulk of the metal and then revealed by milling, or whether these elements were introduced to the trap surface during the ion milling process.

We compare the aluminum Auger spectra measured before and after HEAT 6, when a significant thermal transformation took place, in Fig. 11. We do not observe any significant changes in the aluminum lineshape, indicating that the elemental aluminum surface did not oxidize during this thermal transformation. Also included in Fig. 11 are plots of copper, oxygen and carbon Auger line-shapes measured before and after thermal transformations. We do not observe qualitative changes in any of these lineshapes.

*Ex situ AFM imaging:* The ion trap was removed from vacuum after HEAT 10 and imaged using atomic

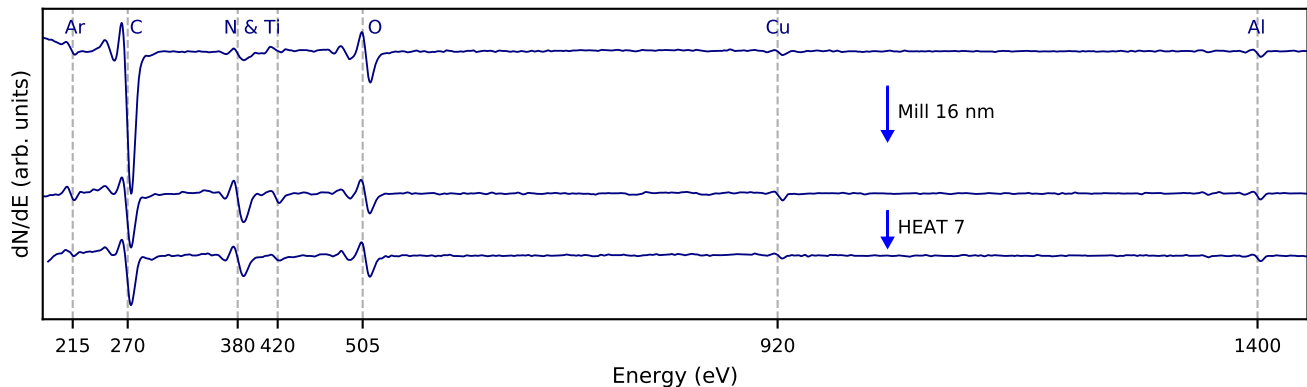


FIG. 8: Auger spectra measured before and after argon ion milling and treatment HEAT 7 show features consistent with the presence of argon, carbon, nitrogen, titanium, oxygen, copper, and aluminum. This milling treatment had a significantly greater impact on the surface composition than the subsequent heat treatment. There is no evidence of new elements emerging during the heat treatment.  $dN/dE$  is the derivative of the magnitude of Auger electron emission with respect to Auger electron energy.

force microscopy (AFM). The results of these measurements are plotted in Fig. 12. As this trap had undergone extensive heat treatments and argon ion milling previous to these measurements, it is referred to in these plots with the label *Treated*. The cross section and RMS roughness of this trap are compared to those of an untreated thin film which was fabricated in an identical manner. This film was stored in atmosphere for several years before the AFM measurements were performed, but it was not milled or heated above room temperature after fabrication. The RMS roughness of the treated film is lower than that of the untreated film on scales smaller than  $0.25 \mu\text{m}^2$ . This is consistent with the comparatively large features that are present in the cross sections of the untreated film, and absent from the cross section of the treated trap, as shown in Fig. 12.

#### IV. ANALYSIS

The parameters of the ten heat treatments discussed in this work, as summarized in Tab. I, are different for each treatment. However, during each heat treatment, the trap was heated to temperatures above 555 K for two or more days, or above 575 K for one or more days. Considering the dynamics of the thermal transformation during the experiments plotted in Fig. 4 and Fig. 5, we expect that each of the ten heat treatments would have generated a thermal transformation had the surface been primed for one. The observed variations in the thermal transformation magnitudes, as plotted in Fig. 3, cannot be explained by variations in heat treatment parameters.

We can investigate why thermal transformations took place during some heat treatments and not others by studying the information contained in the measured Auger spectra. From the surface compositions presented in Fig. 9, and the aluminum lineshapes presented in Fig. 10, it is evident that the composition of the trap

surface was constantly changing throughout the surface treatment experiments. We now compare the evolving chemical state of the aluminum at the surface to the presence and absence of thermal transformations. These features are shown together in Fig. 13.

Thermal transformations did not take place during early heat treatments when the aluminum on the surface of the trap was oxidized, as shown in Fig. 13. As the trap was stored in atmosphere both before and after baking for a cumulative exposure time of 30 weeks, the oxide on the aluminum-copper surface would have been between 2 and 10 nm thick at the start of our experiments. The transformations first occurred during HEAT 5, by which point milling had removed a total of 6.3 nm from the surface, likely breaking through some of the oxide layer to reveal elemental aluminum. During treatment HEAT 6, the surface was primarily composed of elemental aluminum, and the subsequent thermal transformation was significant. Later, when elemental aluminum was replaced by aluminum nitride and aluminum oxide before HEAT 8, the thermal transformations decreased in magnitude and then ceased entirely. Finally, aggressive angled milling before HEAT 10 removed the nitride-oxide layer and re-exposed elemental aluminum, at which point the thermal transformation returned.

Since the occurrence of thermal transformations is correlated with the chemical state of the aluminum at the trap surface, we consider physical processes that are consistent with this pattern. Processes including contaminant deposition, surface oxidation, compound growth, and thermal relaxation of the metal all could take place in a system such as ours. In addition, the specifics of these processes would all be affected by the oxidation or nitrogeneration state of the metal surface. We will now discuss each of these mechanisms in turn, and consider whether any of them can be driving the observed thermal noise transformations.

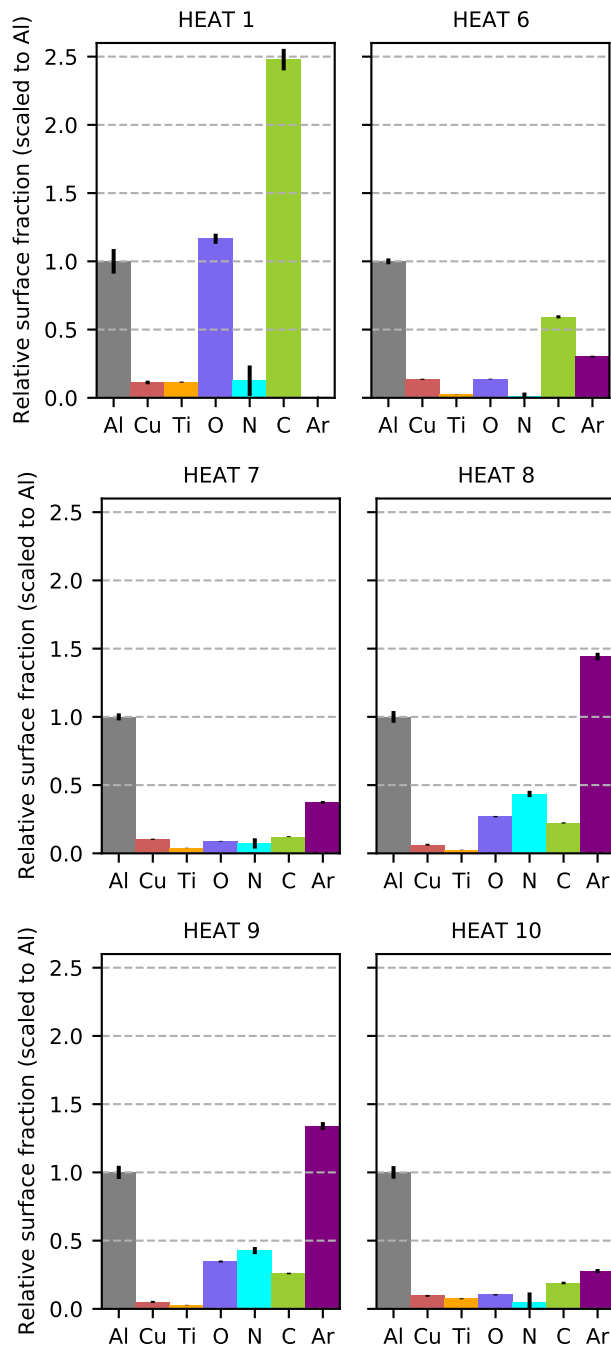


FIG. 9: Relative fractional composition of the trap surface during six heat treatments, scaled such that the aluminum fraction is constant. The trap was milled with argon ions between heat treatments, causing the surface composition to change. These surface composition measurements were completed immediately before the heat treatments indicated, with the exception of the HEAT 9 measurement, which took place immediately after. The Auger spectra from which this data was extracted can be found in App. A.

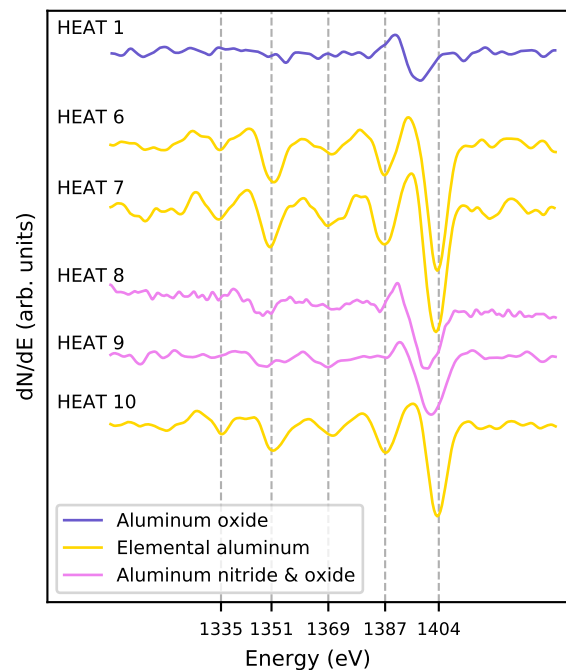


FIG. 10: Measured aluminum Auger spectra. The aluminum line-shape changed as the surface was milled with argon ions. These Auger spectra were taken immediately before the heat treatments indicated, with the exception of the HEAT 9 measurement, which was taken immediately after.

*Contamination level:* Non-metal contaminants are thought to be a major producer of surface electric-field noise, so we first consider whether thermal transformations could be driven by a rise in the contamination level of the trap surface. Elements in the vacuum chamber close to the ion trap heater outgass during a heat treatment, and some of these contaminants may adsorb more readily to elemental aluminum than to aluminum oxide or nitride. Heat can also cause certain elements, in particular carbon, to diffuse from the bulk to the surface of a metal. These elements may diffuse more readily through elemental aluminum than through aluminum oxide or nitride.

A rise in the contaminant level at the trap surface during a thermal transformation should be observable with Auger spectroscopy. When we compare spectra measured before and after a thermal transformation, as shown in Fig. 8, we do not observe signals from any new elements arising after the transformation. In addition, contaminant levels compared before and after three transformations, as shown in Fig. 19, do not exhibit any significant trends. From these measurement results we conclude that the thermal noise transformations are not driven by an increase in the contamination level of the trap surface.

*Chemistry at the trap surface:* Although there are no systematic shifts in the elemental composition of the trap surface during thermal transformations, the heat treatments could be driving changes in the chemical structure

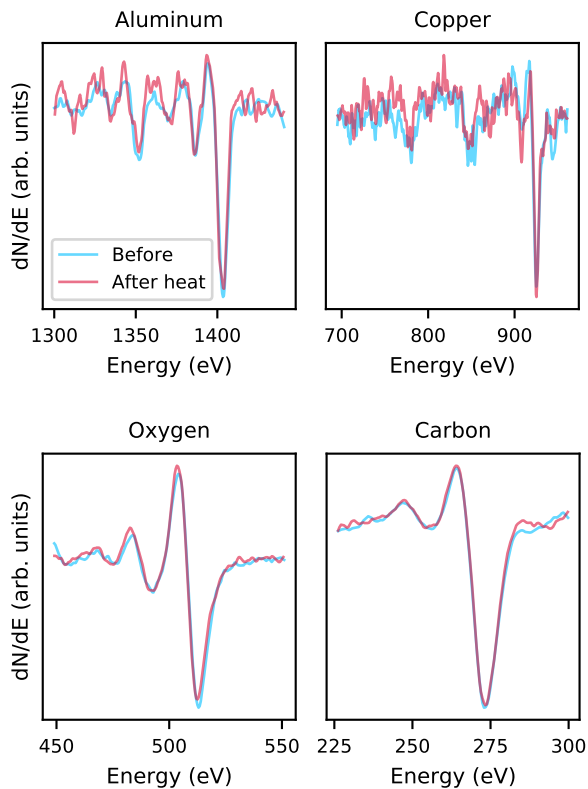


FIG. 11: Auger spectra measured before and after thermal transformations: aluminum in HEAT 6, copper in HEAT 10, oxygen in HEAT 10, carbon in HEAT 7. No thermally-driven line-shape changes are visible. Lines measured before and after heat treatments have been scaled to the magnitude of each element’s largest peak to enable a direct comparison of the overall shape of the spectrum of that element.

of the existing elements. Whether the metal surface participates in these reactions as a catalyst or as a reactant, the oxidation or nitrogenation state of the metal could have a major impact the active chemistry.

Some chemical information can be deduced from the lineshapes of Auger spectra. Thus, a change in one of these lineshapes would indicate that a chemical reaction had taken place. In Fig. 11, we plot aluminum, copper, oxygen and carbon Auger spectra before and after thermal transformations, and find no change in the lineshapes. In particular, we note that the elemental aluminum does not become oxidized or nitrogenated during the heat treatment.

The observed stability of the Auger lineshapes does not rule out chemical changes in general, however, as some chemistry is not visible with Auger spectroscopy. For example, when the incident electron beam from an Auger spectrometer hits the surface of a material, the electrons break up some chemical compounds before their energy signatures can be measured. Hydrocarbon structures are particularly sensitive to energetic electrons [26]. As a result, even if hydrocarbon growth was the driver of a

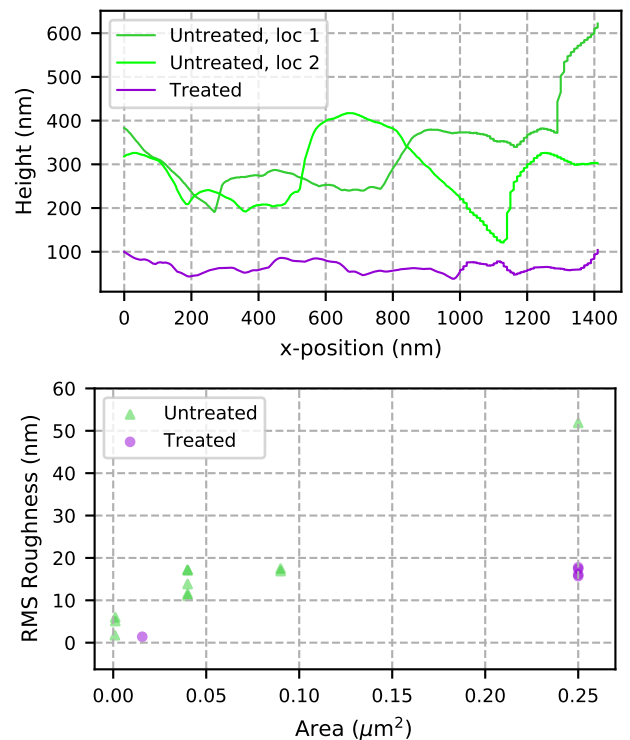


FIG. 12: Cross sections and RMS roughness values corresponding to two metal films. These measurements were performed using atomic force microscopy (AFM). The *Treated* sample refers to ion trap discussed throughout this manuscript. The *Untreated* film was fabricated using the same methods as the ion trap, and never milled or heated above room temperature. The RMS roughness of the untreated trap is higher than that of the heated trap at all measured length scales.

thermal transformation, we might not see evidence of this in any Auger line-shapes. However, if hydrocarbon compound growth drove a rise in ion heating rates, then bombarding these compounds with energetic electrons should cause the heating rates to go back down. We performed electron bombardment after a thermal transformation, see Fig. 7b. The transformation is not reversed by electron bombardment, and thus we conclude that hydrocarbon growth cannot explain the thermally-driven increase of ion heating rates. Instead, electron bombardment slightly increased ion heating rates at high temperatures, which we speculate was caused by the electron-beam-induced deposition of carbon.

*Structural changes of the metal film:* Having found no evidence that chemical reactions are driving thermal noise transformations, we shift our focus to the structure of the metal itself. Elemental aluminum has a melting temperature of 930 K. This is far lower than the melting temperatures of aluminum oxide and aluminum nitride, which are 2340 and 2470 K respectively. If atoms in elemental aluminum are mobile at our heat treatment temperatures of 550 to 600 K, and atoms in aluminum



Atomic restructuring due to thermal relaxation of the metal surface appears to be consistent with the results of our thermal transformation experiments. We next aim to understand how this restructuring may have physically manifested for our metal film. We do not have *in situ* measurements of surface morphology or crystal structure, but we are aided by the observation that ion milling acts in opposition to thermal transformations: thermal noise transformations cause ion heating rates to rise, and milling brings them back down. In addition, after a thermal transformation has saturated, milling can prime the surface for further transformation to take place. We can gain insight into the physics of thermal transformation by considering ways in which milling and heating are known to act in opposition.

The removal of 0.6 nm of material via argon ion milling had a significant impact on noise from a thermally transformed substrate, as shown in Fig. 6b. The subsequent 2 nm of milling reversed nearly the entire effect of the thermal transformation. This is evidence that thermal transformations primarily affect noise originating from or modulated by the top few nanometers of the ion trap surface. Thus, we explore the effects of milling and heating on this length scale.

Milling can disrupt the crystal structure of a thin film by knocking atoms out of their positions in the lattice, and by driving ions and surface adsorbates into the bulk. Milling can also alter the morphology of a surface. Experiments have shown that, under some conditions, ion milling increases the sub-nanometer-scale surface roughness of metals [30, 31]. While our ion trap is primarily composed of aluminum, its surface also contains copper, titanium and non-metal contaminants, all of which are sputtered at different rates. For example, when bombarded with 200 eV argon ions, the sputter rate of aluminum is an order of magnitude greater than that of carbon [32]. In our system, uneven milling of different elements may contribute to an increase in surface roughness at the 1-nm scale during ion milling.

Heating a film such as ours to temperatures above 550 K can affect both the morphology of the film surface and the structure of the bulk crystal [33]. As the metal film is heated, atoms in the bulk gain enough energy to move and reduce strain. Grain boundaries form and move as small crystals merge and form larger crystals. This affects both the bulk of the film and the arrangement of atoms at its surface. In addition, various alloys can form, depending on the local composition of the metal. Given that ion milling is likely to increase disorder in the crystal and add roughness at the 1 nm scale, it is conceivable that heat treatments reverse these effects, thereby increasing the local order of the film.

*Thermally activated fluctuators:* We have discussed the circumstances under which heating rates in our ion trap have gone up (after some heat treatments), and down (after milling). An interesting feature in our data is the uneven effect ion milling can have on heating rates at different temperatures. The most notable example of a

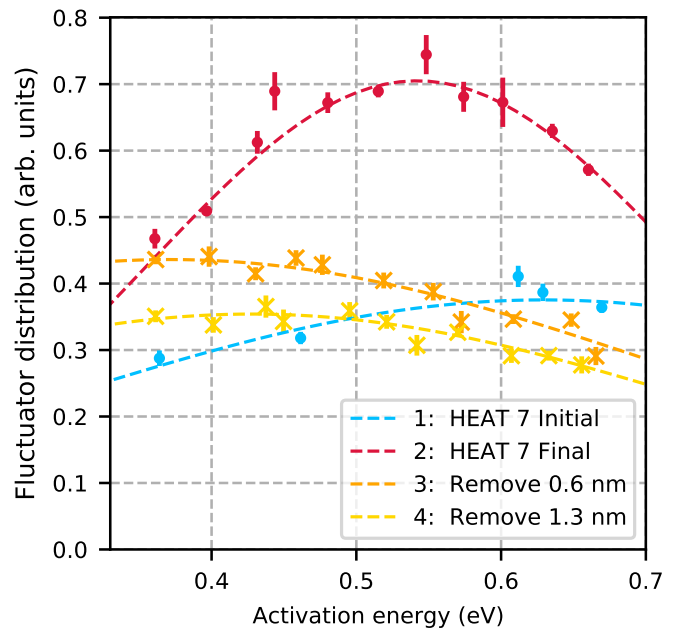


FIG. 14: Thermally activated fluctuator (TAF) distributions extracted ion heating rates measured at a range of different temperatures before and after a thermal transformation and subsequent milling.

surface treatment causing ion heating rates to change by different amounts at different temperatures is the 0.6 nm milling treatment performed after HEAT 7, as shown in Fig. 6b. This argon milling treatment significantly lowered noise at high temperatures, while having very little impact on ion heating rates at room temperature. We can explore this behavior in the context of the thermally activated fluctuator model.

As presented in a previous publication, the noise produced by the surface of this ion trap is consistent with noise from an ensemble of thermally activated fluctuators (TAFs) [18]. In the context of this trap, TAF noise is driven by thermally activated jumps between semi-stable states with different charge configurations. The dynamics of the jumps are determined by the system temperature and the energy barrier between states, while the difference between the electric fields generated by the two states of a single fluctuator determines the magnitude of the electric-field noise that the fluctuator produces.

TAF noise at a fixed temperature and frequency is dominated by a subset of fluctuators with a certain range of activation energies. Thus by measuring ion heating rates at different temperatures, we can map out the relative magnitude of fluctuators with a certain range of energies. We perform these mappings through a procedure described in Ref. [18]. Fluctuator distributions extracted from measurements of ion heating rates taken before and after select surface treatments are shown in Figs. 14 and 15. Additional analysis of these fluctuator distributions can be found in App. C.

When a treatment such as heating or ion milling alters

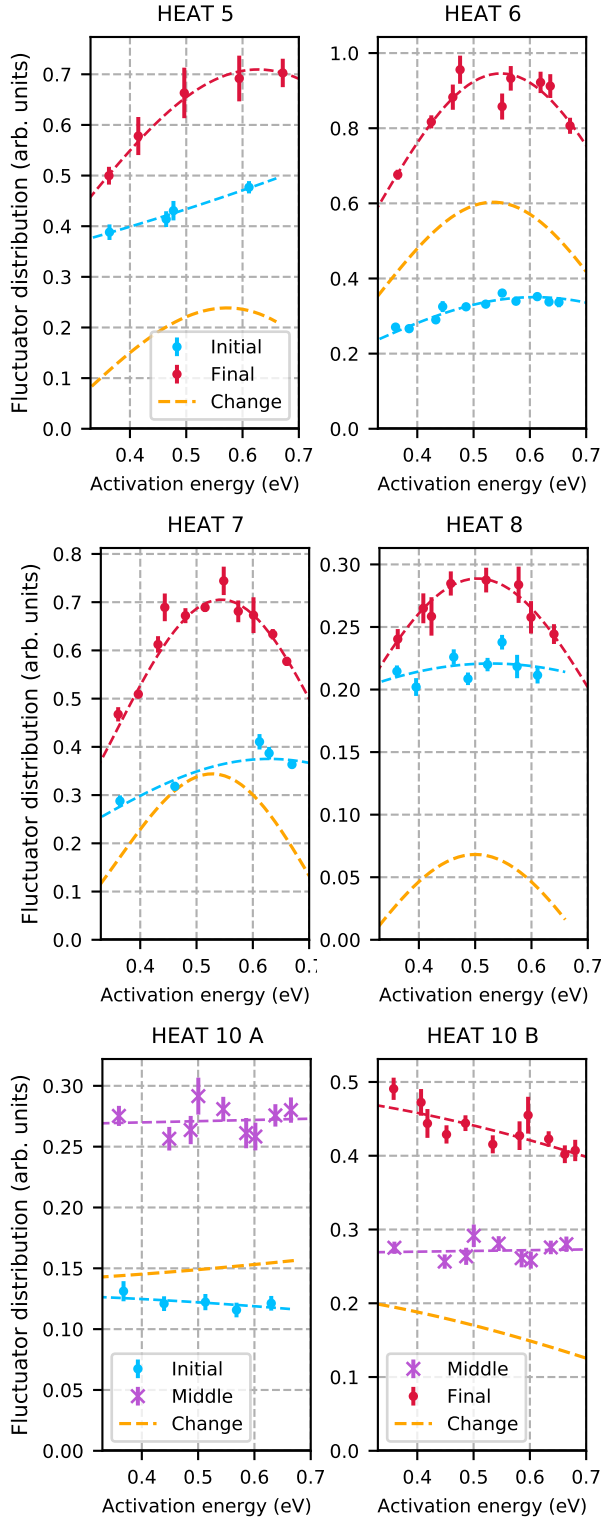


FIG. 15: TAF distributions extracted from ion heating rates measured at a range of different temperatures before and after thermal transformations.

the physical properties of the trap surface, fluctuators with different energies may be affected in different ways. A treatment may selectively add or remove TAFs with

certain activation energies, it may change the activation energies of the existing TAFs, or it may alter the noise magnitude of TAFs with certain energies. It is not surprising then that heating rates at different temperatures are affected differently by surface treatments, as seen in Figs. 14 and 15.

The TAF distributions measured before and after the HEAT 7 thermal transformation are shown in Fig. 14. This heat treatment caused the shape of the TAF distribution to narrow, increase in magnitude, and shift to lower energies such that it peaks around 0.55 eV. Subsequent milling of the surface caused the distribution to widen, decrease in magnitude, and shift to lower energies. Like HEAT 7, treatments HEAT 5, HEAT 6 and HEAT 8 caused the TAF distribution to narrow, increase in magnitude, and shift such that it peaked between 0.5 and 0.6 eV. These distributions are plotted in Fig. 15. The HEAT 10 A and B thermal transformations did not follow the same trend.

## V. DISCUSSION

The ion trap discussed in this work was subjected to alternating heat treatments and argon ion milling treatments. As the trap's surface was milled, the ion heating rate steadily dropped. This drop may be partially explained by a reduction of the contamination level near the surface of the trap as material was removed. Under certain conditions, prolonged heat treatments caused the ion heating rate to rise. These thermal transformations were not accompanied by a rise in contamination levels. The surface also did not oxidize during heat treatments, and we have argued that the thermal noise transformations cannot be explained by hydrocarbon structure growth. Thus, the observed thermal noise transformations cannot be easily explained by a change in the density or chemical structure of contaminants at the trap surface.

The observed temperatures and saturation behaviors of the noise transformations are consistent with a thermal relaxation process driving the rearrangement of atoms on the surface of the metal. Transformations have only taken place when the aluminum at the trap surface was in the elemental state, as opposed to a state of oxidation or nitridation. Atoms in aluminum nitride and aluminum oxide are far less mobile than those in elemental aluminum at temperatures between 500° K and 600° K. These differences in atomic mobility, combined with the observation that the transformations only take place when the aluminum at the surface is elemental, provide evidence that thermal relaxation of the metal is the underlying cause of the thermal noise transformations.

We find that milling and heating act in opposition, with milling both reversing the effects of thermal noise transformations, and also priming the surface for thermal transformations to take place. We speculate that milling reduces noise, in part, by increasing the local disorder near the surface of the metal film, and that heat treat-

ments have the opposite effect. We now discuss physical noise processes that may explain how a locally ordered, recrystallized material could produce more noise than a more amorphous material.

We begin by exploring the significance of TAF distribution changes. We have observed that in many cases, when an ion-milled (presumably disordered) surface is annealed, the TAF distribution narrows and increases in magnitude. This pattern can be seen in Fig. 15. When a thermally transformed (presumably locally ordered) surface is milled, the TAF distribution widens and decreases in magnitude, as shown in 14. One possible explanation for these trends is that TAF energy barriers are generally more homogeneous in an ordered material, and more varied in a disordered material.

In discussing the physical significance of this hypothesis, it is useful to move beyond the mathematical framework of the TAF model, which specifies some features of the dynamics of the noise sources, while being unspecific about their other physical properties. We now consider one possible type of TAF that may be present in our system: non-metal contaminants fluctuating between different binding configurations. In this TAF manifestation, the fluctuator energy barrier is given by the binding energy between the contaminant and the metal. Electric-field noise is generated when the dipole moment of the contaminant changes along with the contaminant-metal binding configuration. The dipole moment can fluctuate when the contaminant moves between lattice sites, when it binds and unbinds at a single site, or when a metal atom at the binding site changes position. Some of these processes are illustrated in Fig. 16.

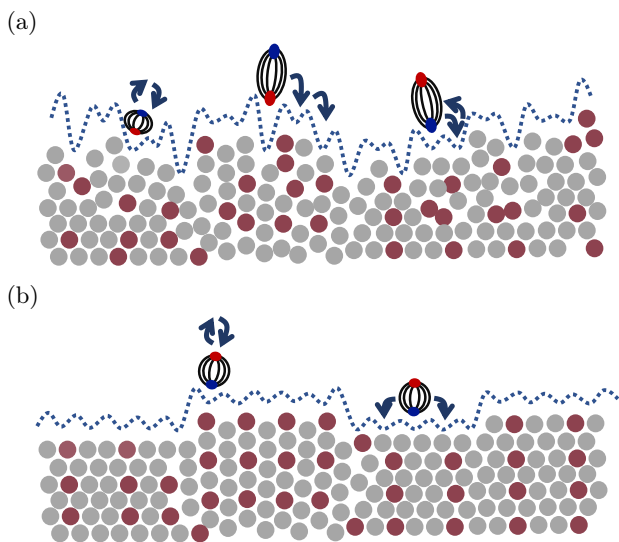


FIG. 16: Illustration of TAF adsorbate dipoles. Cartoons of possible binding-potential landscapes are represented by dotted blue lines. (a) Adsorbate TAFs on a disordered surface. (b) Adsorbate TAFs on a locally ordered (recrystallized) surface.

$1/f$  resistance noise in polycrystalline aluminum films has been linked to TAFs manifesting as defects moving at grain boundaries [34–36]. These TAFs have activation energies that peak in the 0.5 - 1 eV range [34, 37], which is the same energy regime that is relevant to our electric-field noise measurements. Contaminants embedded near the surface of a metal film may produce electric-field noise via the same mechanism, as they fluctuate between different binding configurations. Contaminants embedded in an amorphous film may have a wider range of activation energies than contaminants embedded in the grain boundaries of a recrystallized film. It follows that the TAF distribution of a recrystallized film would have a narrower energy spectrum than the TAF distribution of an amorphous film.

In some simulations, adsorbate binding energies have been found to be stronger in areas with positive curvature (valleys), and weaker in areas with negative curvature (peaks) at cryogenic temperatures [38]. The van der Waals potential of an adsorbate on a surface with sub-nanoscale roughness can increase or decrease by about 50% depending on the local curvature of its binding site. As a consequence, the potential landscape of a rough surface is more varied than that of a smooth surface. The variability of this landscape will also be affected by the distribution of impurities. Cartoon illustrations of potential landscapes of ordered and disordered surfaces are shown in Fig. 16. If TAF energy barriers correspond directly to adsorbate-surface binding energies, then the TAF distribution of a contaminated, crystalline surface should be composed of peaks at a discrete set of energies characteristic of the structure of the lattice and the nature of the adsorbates. When this surface becomes rough and disordered, a wider range of binding sites becomes available, causing the TAF distribution peaks to widen and reduce in magnitude.

There is yet another way that changes in the surface potential landscape could affect the electric-field noise magnitude: by changing the correlation length of the noise process. A group of noise sources fluctuating in phase with each other produces more noise than the same group of noise sources fluctuating independently. Heat-induced atomic restructuring may increase the noise correlation length in our trap and lead to larger heating rates.

As discussed previously, a disordered surface can have large variations in adsorbate-metal binding energies. Surface roughness, for example, may shield nearby noise sources from interacting with each other, leading to small spatial noise correlating lengths. In contrast, smooth crystal facets contain arrays of well-defined, periodic binding sites, enabling the build-up of correlations between fluctuating adsorbates (see Fig. 17 for a cartoon depiction). Noise magnitudes grow in proportion with the square of the noise correlation length (or equivalently with the area of a fluctuating patch) for a constant surface coverage provided the correlation length is much smaller than the ion-surface separation [39, 40]. To raise

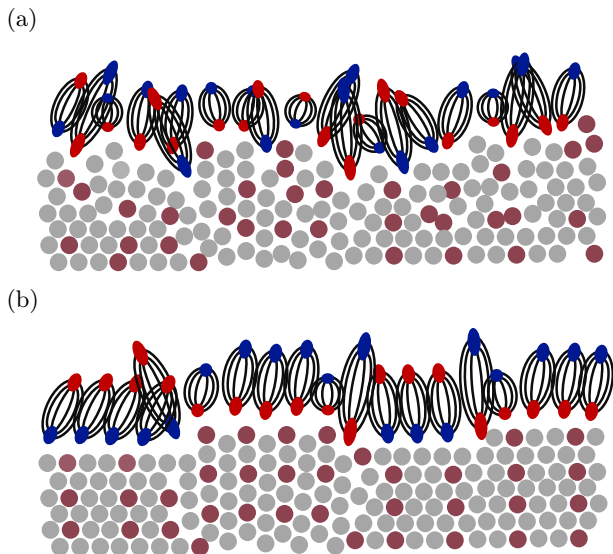


FIG. 17: Cartoon of (a) uncorrelated noise sources on a disordered surface (b) correlated noise sources on a locally ordered surface.

the noise in an ion trap by a factor of three, as observed during the HEAT 10 thermal transformation, the TAF correlation length would need to rise by a factor of  $\sqrt{3}$ .

Thermally-activated fluctuations correlated over full nanocrystals have been observed experimentally in resistance noise measurements [41]. Further theoretical work will be critical to determining whether or not electric-field-noise-producing surface TAFs can become similarly correlated.

## VI. CONCLUSION

In a series of experiments performed on a single ion trap, we observed that ion heating rates can rise as a result of an *in situ* heat treatment. In an effort to illuminate the underlying physics of this thermal transformation, we studied and characterized this process using ion milling, electron bombardment, heat treatments, Auger spectroscopy, and ion heating rate measurements.

To characterize the timescale and temperature dependence of the transformation, we held the trap at elevated temperatures while repeatedly measuring ion heating rates. In one experiment we found the transformation to saturate on a timescale of 1.6 days at 575 K. Secondary transformations were observed at higher temperatures.

Argon ion milling treatments altered the composition of the trap surface, and we tracked these changes in composition with Auger spectroscopy. We found a correlation between the behavior of thermal transformations and the chemical state of the aluminum on the trap surface: when the aluminum was in the elemental form, the noise transformed in response to a heat treatment. When the aluminum was oxidized or nitrogenized, no transformation

took place.

Auger spectra taken before and after thermal transformations allow us to rule out contaminant deposition as the underlying driver of the rise in noise. Auger spectra combined with electron bombardment treatments allow us to discount, though not entirely rule out, chemical changes.

All of the measured properties of the thermal noise transformations are consistent with atomic restructuring taking place near the surface of the trap. After discussing how sub-nanoscale atomic structures evolve with milling and heating, we conjecture that in this specific trap, heat treatments can raise ion heating rates through local ordering of the surface, and that milling resets this transformation by roughing up and disordering the surface. The observed relationship between sub-nanoscale disorder and electric-field noise may be linked to variations in adsorbate binding energies, dynamics of embedded contaminants, and the extent of spatial noise correlations.

Thermal transformations caused heating rates in our ion trap to rise, as measured at temperatures between 300 K and 600 K. However, if the temperature dependencies of the heating rates are extrapolated outward, we see hints that thermal transformations may improve the noise performance of traps operated at lower temperatures. We have speculated that an increase in disorder at the trap surface reduces the noise levels of traps operated at room temperature, yet a locally ordered surface may be more beneficial for traps in cryogenic environments. This may explain why milling has increased noise at cryogenic temperatures in some traps [11]. Our work highlights the importance of designing trap fabrication processes that are optimized for the operating temperatures of the ion traps.

We acknowledge Ben Saarel and Keith Ray for manuscript review and helpful conversations. We also acknowledge Arthur Nelson for providing insight into surface science and Adam Udi for assistance with software development. Part of the trap fabrication was performed in the UC Berkeley Marvell Nanofabrication Laboratory. M.B.-U. acknowledges an NSF Graduate Research Fellowship. Part of this work was performed under the auspices of the U.S. Department of Energy by Lawrence Livermore National Laboratory under Contract DE-AC52-07NA27344.

## Appendix A: Auger spectroscopy

We reported, in Fig. 9, the elemental composition of the ion trap surface at various times throughout a series of surface treatment experiments. The full measured Auger spectra from which these compositions were extracted are presented in Fig. 18. All measurements were performed *in situ*, as in vacuum was not broken between surface treatments and Auger spectroscopy measurements.

In comparing Auger spectra measured before and after

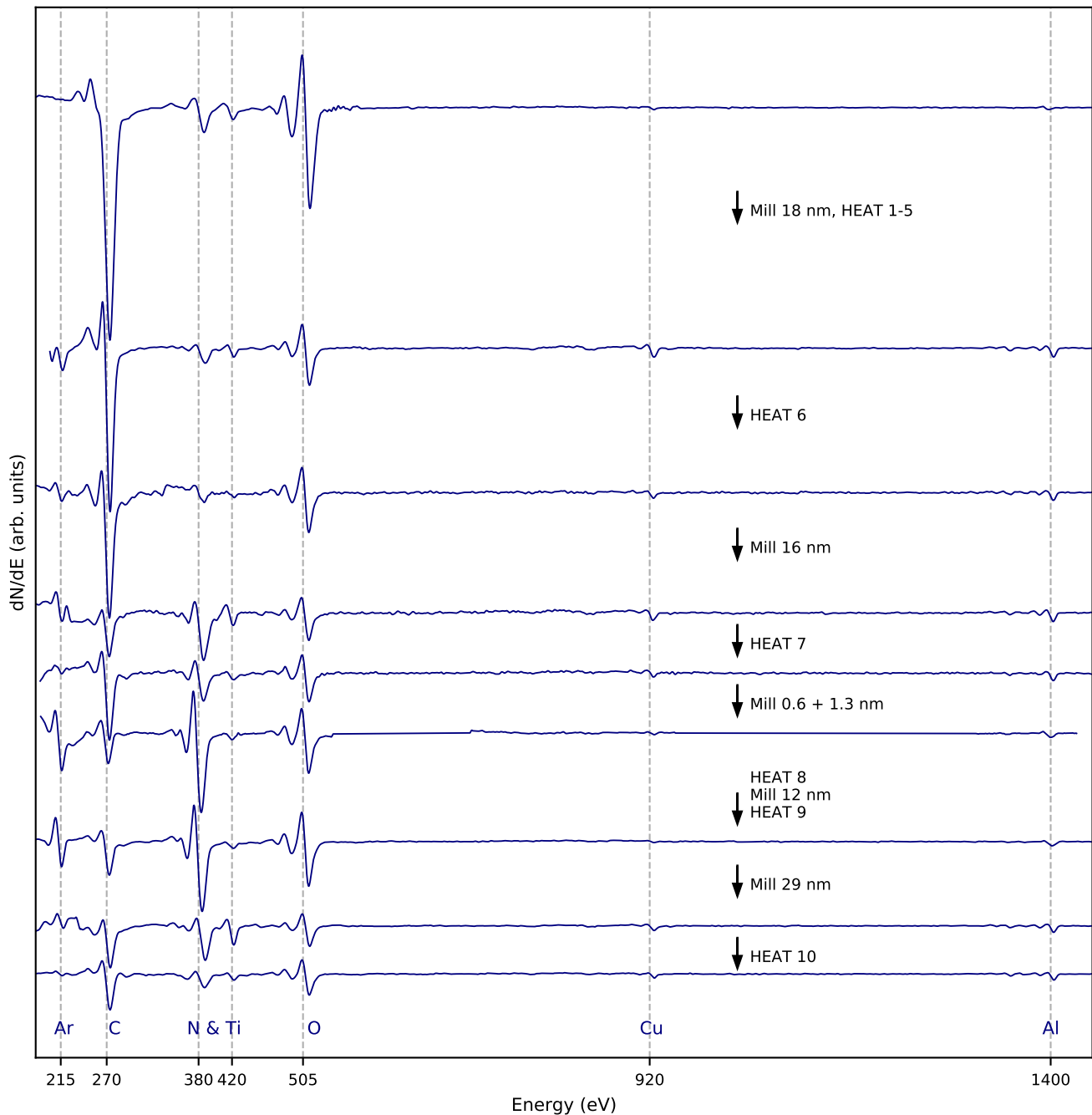


FIG. 18: Data from Auger spectroscopy measurements performed *in situ* on the ion trap. Before plotting and analysis was performed, large-scale magnitude drifts were subtracted out. Features identified as characteristic peaks of specific elements are labeled. Notes on heating and milling describe the surface treatments that were performed between Auger spectroscopy measurements.

argon ion milling, it is evident that the composition of the ion trap surface changed significantly as a result of milling. In contrast, the relative peak magnitudes were much less affected by heat treatments. The relative surface fractions of identified elements are compared before and after three heat treatments in Fig. 19. There are no consistent, statistically significant trends in the surface composition changes that took place before and after

thermal transformations. Small variations between measurements are expected as each scan was performed on a slightly different location on the substrate.

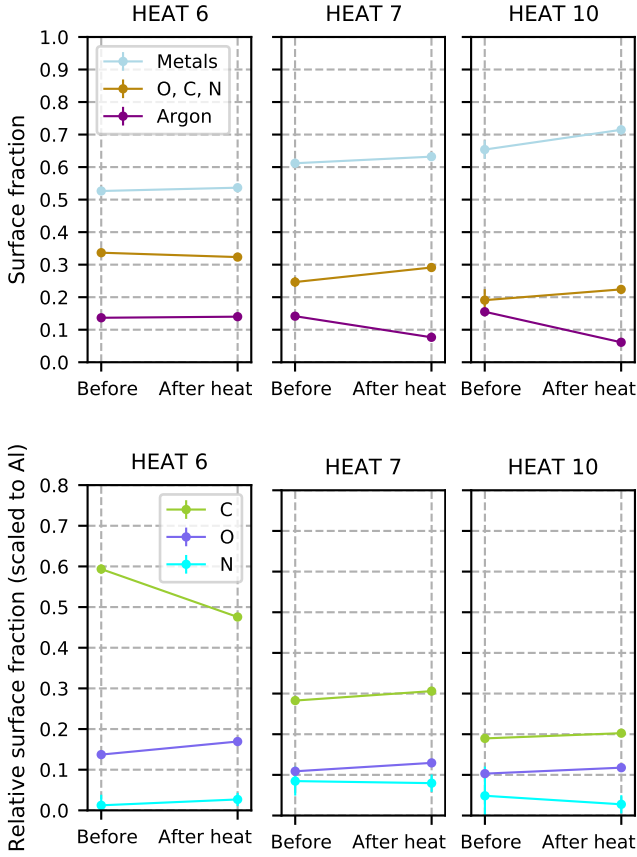


FIG. 19: Surface fractions measured before and after thermal transformations. Metals includes aluminum, copper and titanium. In the lower three plots, carbon, oxygen and nitrogen are scaled relative to aluminum. We observe no statistically significant trends. The Auger spectra from which these surface compositions were extracted can be found in App. A.

### Appendix B: Surface treatments

We have discussed how the behavior of an ion trap was affected by ten heat treatments. In Fig. 20 we present the details of these heat treatments, plotting how the temperature of the ion trap varied as a function of time.

The ion trap was milled between each heat treatment. In some cases the trap was milled multiple times between these heat treatments, or bombarded with electrons at the ion-heating-rate measurement region. After each milling step or electron treatment, the temperature dependence of the ion heating rates was measured. These measurements were performed more quickly and at lower temperatures than those reached during heat treatments.

The parameters of all argon ion milling surface treatments can be found in Tab. II. This table describes the milling treatments and electron bombardments in chronological order. This chronology also includes the ten heat treatments to provide the necessary context as to when these treatments were performed. Additional in-

formation on the full trap history can be found in Ref [42].

TABLE II: Chronology of argon ion milling, electron bombardment, and heat treatments, with details of milling parameters.

Treatment	Energy deposited (J/cm <sup>2</sup> )	Beam Angle	Beam Energy (eV)
HEAT 1	—	—	—
Mill 0.13 nm	0.1	normal	200
HEAT 2	—	—	—
Mill 0.13 nm	0.1	normal	200
HEAT 3	—	—	—
Mill 0.6 nm	0.5	normal	200
HEAT 4	—	—	—
Mill 1.5 nm	1.2	normal	200
Mill 3.9 nm	2.9	normal	400
HEAT 5	—	—	—
Mill 11.4 nm	7.5	normal	400
HEAT 6	—	—	—
Mill 16.4 nm	8.8	normal	200
HEAT 7	—	—	—
Mill 0.6 nm	0.2	normal	200
Mill 1.3 nm	0.6	normal	200
Electron treat	—	—	—
HEAT 8	—	—	—
Mill 12.2 nm	4.9	normal	200
HEAT 9	—	—	—
Electron treat	—	—	—
Mill 18.9 nm	9.7	45°	400
Mill 9.8 nm	5.2	45°	500
HEAT 10	—	—	—
Electron treat	—	—	—

### Appendix C: Thermally activated fluctuators

The results of the first ion heating rate measurements performed in this trap were consistent with the thermally activated fluctuator (TAF) model, as discussed in a previous publication [18]. Additional heating rate measurements were performed as the trap was subsequently milled, heated, and bombarded with electrons. In this manuscript, we have presented thirteen TAF distributions extracted from data taken as part of these surface treatment experiments. We will now review how to evaluate the applicability of the TAF model to a given set of ion heating rate measurements, and report a quantitative analysis of our data in the context of this model.

The temperature scaling corresponding to a distribution of TAFs will never include features sharper than the width of an individual fluctuator, as illustrated in [18]. Beyond this requirement, the TAF model does not predict a functional form for how noise from a generic distribution of fluctuators should scale with temperature. Instead, this model establishes that there is a specific relationship between the temperature scaling and frequency scaling of TAF noise.

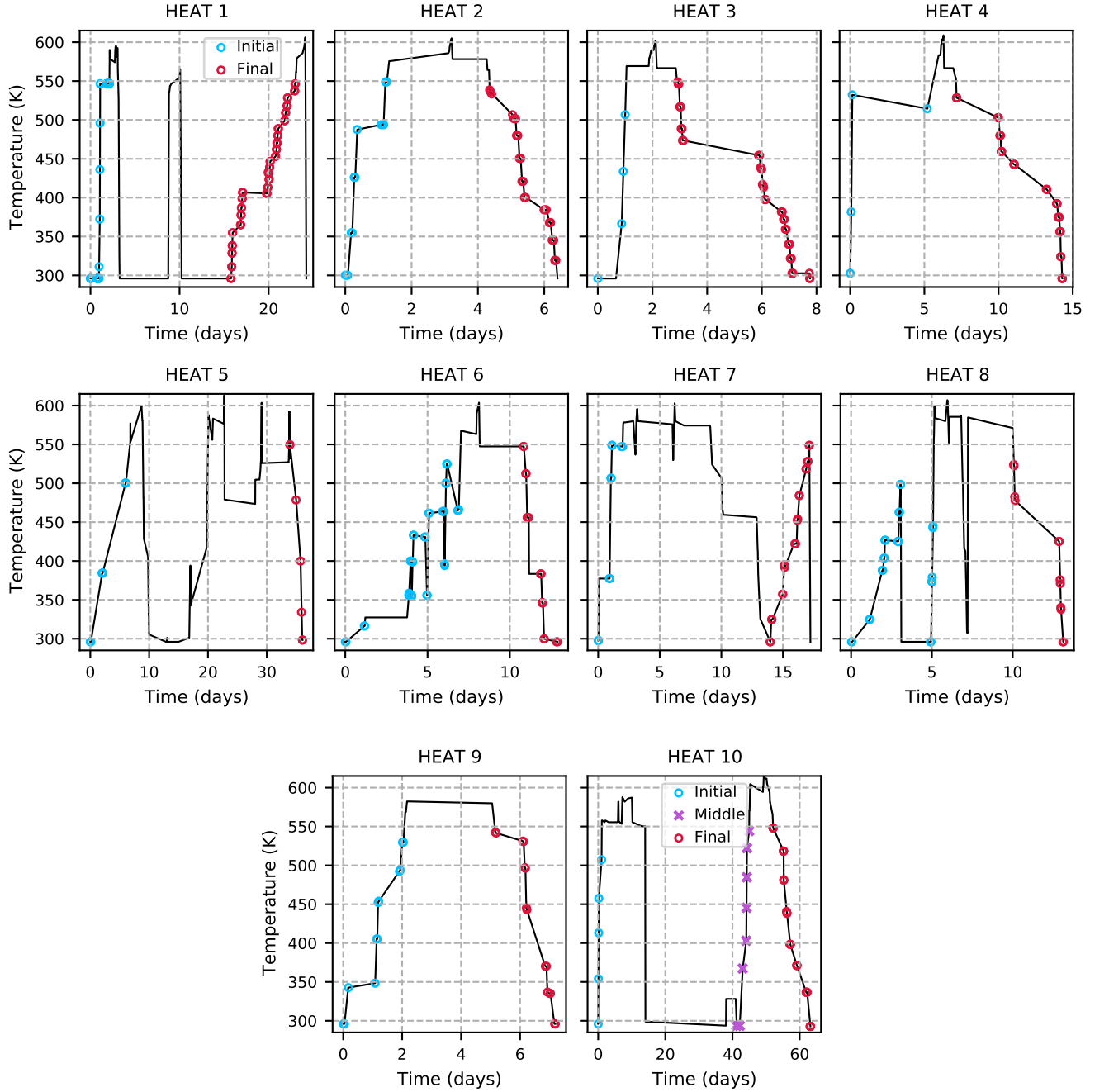


FIG. 20: The timing and temperatures of ten heat treatments performed on the ion trap. In Fig. 3 ion heating rates were reported as a function of temperature, and labelled as *initial*, *middle*, or *final*. The points marked here, and labeled in the same manner, indicate in more detail the context surrounding the ion heating rate measurements reported in Fig. 3.

TAF noise from a slowly-varying distribution of fluctuators scales inversely with frequency, locally, according to:

$$S(\omega) \propto 1/\omega^\alpha \quad (\text{C1})$$

where  $\alpha$  is the frequency scaling exponent, and the measurement frequency  $\omega$  is equal to the secular frequency of the ion. The TAF model predicts that  $\alpha$  will depend on

the slope of the temperature scaling according to [43]:

$$\alpha(\omega, T) = 1 - \frac{1}{\ln(\omega\tau_0)} \left( \frac{\partial \ln S}{\partial \ln T} - 1 \right). \quad (\text{C2})$$

Before we use the TAF model to make predictions about the scaling behavior of our heating rate measurements, certain measurements are excluded that are

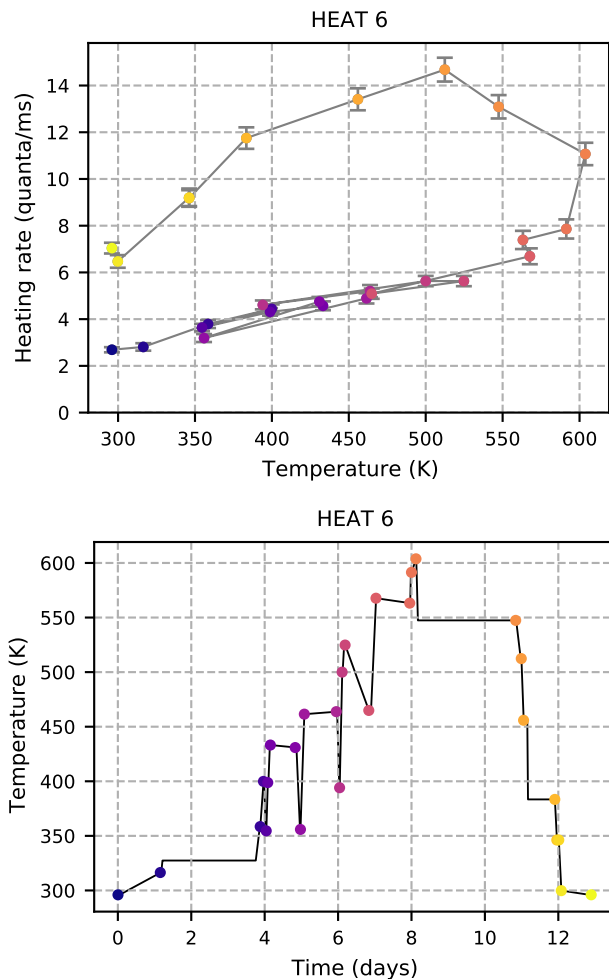


FIG. 21: During treatment HEAT 6, ion heating rates were measured as the trap temperature was raised and lowered in an alternating manner. No thermal transformation took place until after the temperature had been raised above 550 K. These measurements were performed at trap frequency  $2\pi \times 0.88$  MHz.

known to be outside of this model, such as those taken during active thermal transformations. Although noise during an active transformation may still be dominated by TAFs, temperature-scaling slopes and frequency-scaling exponents lose physical significance when each measurement samples a different underlying TAF distribution. We performed an experiment to determine at what temperatures thermal transformations begin to take place. The results of this experiment are shown in Fig. 21, where data from HEAT 6 are plotted. During the first seven days of this heat treatment, we alternated between raising and lowering the temperature of the substrate between measurements. During this portion of the experiment, ion heating rates increased as the temperature was raised, and they decreased back to previously-measured values when the temperature was lowered. The transformation did not take place until the temperature

of the trap was raised above 550 K. With this in mind, we have chosen to exclude all data taken above 550 K. This also removes the feature in which the heating rates abruptly increase in magnitude, as was shown in Fig. 2. This high-temperature shoot off is not consistent with TAF noise.

After high-temperature data is excluded, the data is binned and averaged in 10 K increments. Then, we fit a Gaussian to each heating-rate temperature dependence to obtain noise distributions with smoothly-varying slopes. The choice to use a Gaussian fit is not a statement about the underlying physics of this system; it is simply versatile enough to fit the data of interest.

In order to use the smoothed heating-rate temperature dependence to make a prediction of how  $\alpha$  scales with temperature, a value must be chosen for the attempt time  $\tau_0$ . In the context of defect dynamics in solid state systems, attempt times between  $10^{-12}$  and  $10^{-14}$  s have been used, as this is on the order of the inverse phonon frequency [34, 44, 45]. Attempt times on the same order have been used in the context of adatom diffusion on metal surfaces [46]. Defect fluctuations and adsorbate motion are both viable candidates for the physical manifestation of TAFs in our system, so we perform our analysis using an attempt time of  $10^{-13}$  s. The dependence of  $\alpha$  on  $\tau_0$  is logarithmic, so it is not critical to know the precise value of  $\tau_0$ .

To evaluate whether or not the noise produced by our ion trap is consistent with the TAF model, we measure ion heating rates as a function of temperature at two frequencies. The slope of each heating-rate temperature dependence is analyzed in the context of the TAF model to predict the temperature dependence of  $\alpha$ . Measurements of  $\alpha$  are extracted at each temperature at which heating rates were measured at multiple frequencies, assuming the heating rate scales with frequency according to Eq. 2. These extracted  $\alpha$  values are compared to the  $\alpha$  predictions.

It follows from Eq. C2 that if the slope of the temperature scaling changes with temperature, so does  $\alpha$ . Fig. 22 includes a heating-rate temperature dependence with a slope that decreases as a function of temperature (HEAT 7 final), and a heating-rate temperature dependence with a constant slope (HEAT 10 final). As predicted by the TAF model,  $\alpha$  decreases as the temperature rises during HEAT 7 final. As predicted, this trend in  $\alpha$  is not observed in HEAT 10 final.

TAF distributions extracted from heating-rate temperature dependencies measured at different frequencies are slightly offset from each other in energy. In both datasets plotted in Fig 22, the 0.88 and 1.3 MHz TAF distributions match in regions where the activation energies overlap, which indicates that these measurements are consistent with TAF noise. This observation is equivalent to the statement that  $\alpha$  values are consistent with TAF predictions.

To determine the quantitative accuracy of the TAF prediction, we perform a  $\chi^2$  analysis comparing the mea-

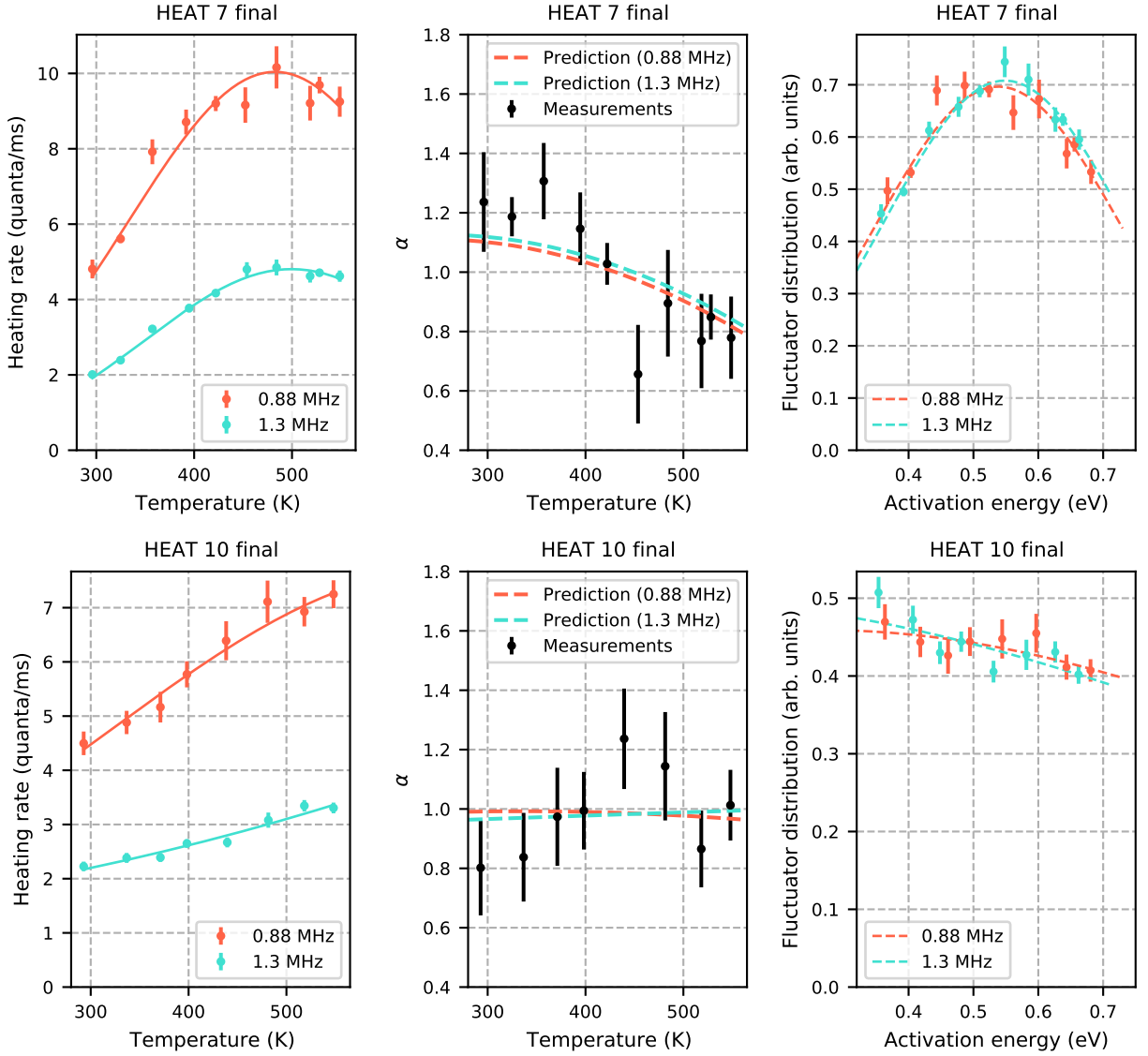


FIG. 22: Left: the temperature dependence of ion heating rates measured at two frequencies during HEAT 7 final and HEAT 10 final. Center: the measured  $\alpha$  values plotted alongside the TAF model predictions extracted from the slopes of the temperature dependencies. Right: TAF distributions extracted from the corresponding heating-rate temperature dependencies.

sured values of  $\alpha$  to the predictions from the TAF model extracted from the Gaussian fit of the  $2\pi \times 1.3$  MHz heating-rate temperature dependence. The  $\chi^2$  values are calculated as follows:

$$\chi^2 = \sum_{i=1}^n \left( \frac{\alpha_i - \alpha_{\text{TAF}}(T_i)}{\sigma_i} \right)^2 \quad (\text{C3})$$

where  $\alpha_i$  is a direct measurement of the frequency scaling exponent,  $\sigma_i$  is the standard error of  $\alpha_i$ , and  $T_i$  is the temperature at which  $\alpha_i$  was measured.  $\alpha_{\text{TAF}}(T_i)$  is the value of  $\alpha$  at temperature  $T_i$  predicted by the TAF model using one of the measured temperature dependencies.  $n$  is the total number of  $\alpha$  measurements in this

data-set. The p-value of this data-set is determined from the  $\chi^2$  value, using the number of  $\alpha$  measurements  $n$  as the number of degrees of freedom.

In this manuscript, we have reported TAF distributions corresponding to thirteen different heating-rate temperature-dependence measurements. In three of these experiments, we measured the temperature dependence of the ion heating rates at either 1.3 MHz or 0.88 MHz, but not both. The other ten experiments included measurements of heating-rate temperature dependencies at both of these frequencies, which allows us to calculate  $\alpha$  measurements as a function of temperature. In Fig. 23 we plot the TAF predictions and  $\alpha$  measurements corresponding to these ten experiments. The results of our quantitative analysis are reported in

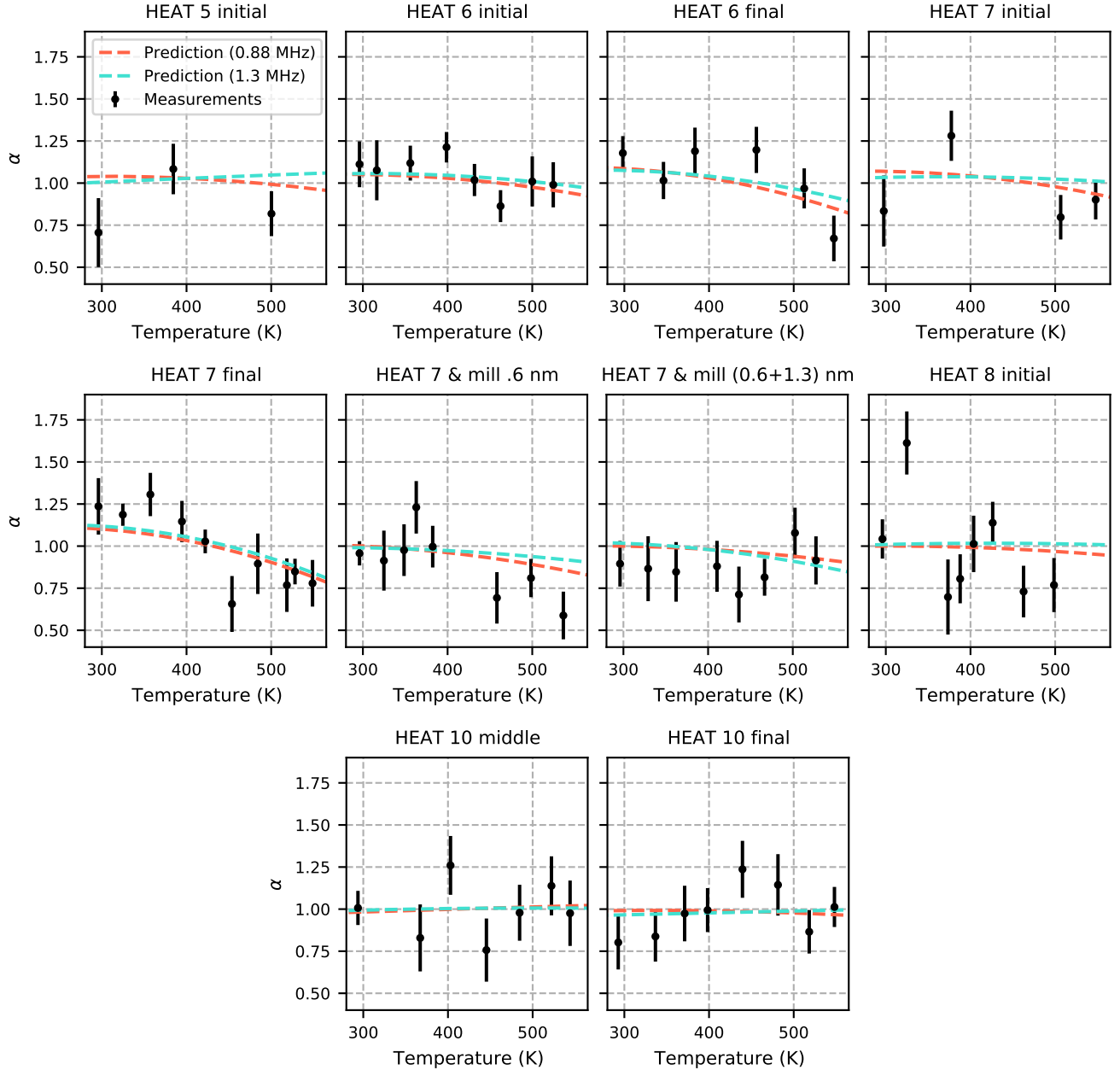


FIG. 23: Direct measurements of the temperature scaling exponent  $\alpha$  compared to predictions from the TAF model. These predictions are extracted from the slopes of the measured heating-rate temperature dependencies.

Tab. III.

The p-values reported in Tab. III are greater than 0.1 for nine out of ten of the analyzed data sets. This indicates that these nine data sets are all consistent with the TAF model. The experiment HEAT 8 INITIAL had a p-value of 0.01 when compared with the TAF prediction, but on further analysis we find that it also has a p-value of 0.01 when compared to a linear fit of  $\alpha$  measurements as a function of temperature. These low p-values can be explained by the large scatter of the  $\alpha$  measurements. The large scatter of these  $\alpha$  measurements indicates that our

measurement process contains sources of error that are not accounted for in the reported error bars. Perhaps the most significant sources of measurement error in our system are intermittent fluctuations of laser frequencies and powers. A concerted effort is made to stabilize and monitor the measurement and cooling lasers, but brief laser instabilities occasionally affect the ion heating rates. For this reason, we will not rule out TAF as a relevant model in HEAT 8 INITIAL.

The TAF model is able to successfully predict the magnitude and temperature dependence of  $\alpha$  values measured in our system. This observation has led us to using the

TABLE III: Quantitative analysis of fit to thermally activated fluctuator model.

Treatment	Number of $\alpha$ measured	$\chi^2$	p-value
HEAT 5 initial	3	5.3	0.15
HEAT 6 initial	8	6.9	0.55
HEAT 6 final	6	7.5	0.28
HEAT 7 initial	4	7.4	0.12
HEAT 7 final	10	10.5	0.40
HEAT 7 & mill .6 nm,	8	12.7	0.12
HEAT 7 & mill (.6+1.3) nm	8	7.3	0.50
HEAT 8 initial	8	21.2	0.01
HEAT 10 middle	7	5.3	0.62
HEAT 10 final	8	5.8	0.67

TAF model as a tool with which to interpret our data. However, the TAF model is a mathematical framework that describes a highly simplified physical system. It does not specify the precise details of the underlying microscopic processes. There may be other physical models that can describe some or all of our observations, in a way that either supplements or supplants the TAF model.

- [1] M. Brownnutt, M. Kumph, P. Rabl, and R. Blatt, Ion-trap measurements of electric-field noise near surfaces, *Reviews of Modern Physics* **87**, 1419 (2015).
- [2] K. R. Brown, J. Chiaverini, J. Sage, and H. Häffner, Materials Challenges for Trapped-Ion Quantum Computers, arXiv: 2009.00568 [quant-ph] (2020).
- [3] M. Kim, H. J. Mamin, M. H. Sherwood, K. Ohno, D. D. Awschalom, and D. Rugar, Decoherence of Near-Surface Nitrogen-Vacancy Centers Due to Electric Field Noise, *Physical Review Letters* **115**, 87602 (2015).
- [4] B. A. Myers, A. Ariyaratne, and A. C. Jayich, Double-Quantum Spin-Relaxation Limits to Coherence of Near-Surface Nitrogen-Vacancy Centers, *Physical Review Letters* **118**, 197201 (2017).
- [5] E. Paladino, Y. M. Galperin, G. Falci, and B. L. Altshuler,  $1/f$  noise: Implications for solid-state quantum information, *Reviews of Modern Physics* **86**, 361 (2014).
- [6] B. G. Christensen, C. D. Wilen, A. Opremcak, J. Nelson, F. Schlenker, C. H. Zimonick, L. Faoro, L. B. Ioffe, Y. J. Rosen, J. L. Dubois, B. L. Plourde, and R. McDermott, Anomalous charge noise in superconducting qubits, *Physical Review B* **100**, 140503 (2019).
- [7] S. Kafanov, H. Brenning, T. Duty, and P. Delsing, Charge noise in single-electron transistors and charge qubits may be caused by metallic grains, *Physical Review B - Condensed Matter and Materials Physics* **78**, 125411 (2008).
- [8] J. L. Garrett, D. Somers, and J. N. Munday, The effect of patch potentials in Casimir force measurements determined by heterodyne Kelvin probe force microscopy, *Journal of Physics Condensed Matter* **27**, 1 (2015).
- [9] F. Antonucci, A. Cavalleri, R. Dolesi, M. Hueller, D. Nicolodi, H. B. Tu, S. Vitale, and W. J. Weber, Interaction between stray electrostatic fields and a charged free-falling test mass, *Physical Review Letters* **108**, 10.1103/PhysRevLett.108.181101 (2012).
- [10] M. Armano, H. Audley, G. Auger, J. T. Baird, P. Binetruy, M. Born, D. Bortoluzzi, N. Brandt, A. Bursi, M. Caleno, A. Cavalleri, A. Cesarini, M. Cruise, K. Danzmann, M. d. D. Silva, I. Diepholz, R. Dolesi, N. Dunbar, L. Ferraioli, V. Ferroni, E. D. Fitzsimons, R. Flatscher, M. Freschi, J. Gallegos, C. G. Marirrodriga, R. Gerndt, L. Gesa, F. Gibert, D. Giardini, R. Giusteri, C. Grimalani, J. Grzysch, I. Harrison, G. Heinzel, M. Hewitson, D. Hollington, M. Hueller, J. Huesler, H. Inchauspé, O. Jennrich, P. Jetzer, B. Johlander, N. Karnesis, B. Kaune, C. J. Killow, N. Korsakova, I. Lloro, L. Liu, R. Maarschalkerweerd, S. Madden, D. Mance, V. Martín, L. Martin-Polo, J. Martino, F. Martin-Porqueras, I. Mateos, P. W. McNamara, J. Mendes, L. Mendes, A. Moroni, M. Nofrarias, S. Paczkowski, M. Perreux-Lloyd, A. Petiteau, P. Pivato, E. Plagnol, P. Prat, U. Ragnit, J. Ramos-Castro, J. Reiche, J. A. R. Perez, D. I. Robertson, H. Rozemeijer, F. Rivas, G. Russano, P. Sarra, A. Schleicher, J. Slutsky, C. Sopena, T. J. Sumner, D. Texier, J. I. Thorpe, C. Trenkel, D. Vetrugno, S. Vitale, G. Wanner, H. Ward, P. J. Wass, D. Wealthy, W. J. Weber, A. Wittchen, C. Zanoni, T. Ziegler, and P. Zweifel, Charge-induced force-noise on free-falling test masses: results from LISA Pathfinder, *Physical Review Letters* **118**, 10.1103/PhysRevLett.118.171101 (2017).
- [11] J. A. Sedlacek, J. Stuart, D. H. Slichter, C. D. Bruzewicz, R. McConnell, J. M. Sage, and J. Chiaverini, Evidence for multiple mechanisms underlying surface electric-field noise in ion traps, *Physical Review A* **98**, 63430 (2018).
- [12] D. T. C. Allcock, L. Guidoni, T. P. Harty, C. J. Ballance, M. G. Blain, A. M. Steane, and D. M. Lucas, Reduction of heating rate in a microfabricated ion trap by pulsed-laser cleaning, *New Journal of Physics* **13**, 123023 (2011).
- [13] N. Daniilidis, S. Gerber, G. Bolloten, M. Ramm, A. Ransford, E. Ulin-Avila, I. Talukdar, and H. Häffner, Surface noise analysis using a single-ion sensor, *Physical Review B* **89**, 245435 (2014).
- [14] D. A. Hite, Y. Colombe, A. C. Wilson, K. R. Brown, U. Warring, R. Jördens, J. D. Jost, K. S. McKay, D. P. Pappas, D. Leibfried, and D. J. Wineland, 100-Fold Reduction of Electric-Field Noise in an Ion Trap Cleaned with In Situ Argon-Ion-Beam Bombardment, *Physical Review Letters* **109**, 103001 (2012).
- [15] K. S. McKay, D. A. Hite, Y. Colombe, R. Jördens, A. C. Wilson, D. H. Slichter, D. T. C. Allcock, D. Leibfried, D. J. Wineland, and D. P. Pappas, Ion-trap electrode preparation with  $\text{Ne}^{8+}$  bombardment, arXiv:1406.1778v1 (2014).
- [16] R. McConnell, C. Bruzewicz, J. Chiaverini, and J. Sage, Reduction of trapped-ion anomalous heating by in situ surface plasma cleaning, *Physical Review A* **92**, 020302

- (2015).
- [17] E. Kim, A. Safavi-Naini, D. A. Hite, K. S. McKay, D. P. Pappas, P. F. Weck, and H. R. Sadeghpour, Electric-field noise from carbon-atom diffusion on a Au(110) surface: First-principles calculations and experiments, *Physical Review A* **95**, 033407 (2017).
- [18] C. Noel, M. Berlin-Udi, C. Matthiesen, J. Yu, Y. Zhou, V. Lordi, and H. Häffner, Electric-field noise from thermally activated fluctuators in a surface ion trap, *Physical Review A* **99**, 063427 (2019).
- [19] K. G. Ray, B. M. Rubenstein, W. Gu, and V. Lordi, Van Der Waals-corrected density functional study of electric field noise heating in ion traps caused by electrode surface adsorbates, *New Journal of Physics* **21**, 053043 (2019).
- [20] C. F. Roos, *Controlling the quantum state of trapped ions*, Ph.D. thesis, University of Innsbruck (2000).
- [21] See the Berlin-Udi dissertation [42] for more discussion of heating rates measured in this trap above 550 K. This dissertation also contains additional information about the trap geometry, measurement methods, analysis techniques, and the experimental setup.
- [22] J. F. Ziegler, M. D. Ziegler, and J. P. Biersack, SRIM - The stopping and range of ions in matter (2010), *Nuclear Instruments and Methods in Physics Research, Section B: Beam Interactions with Materials and Atoms* **268**, 1818 (2010).
- [23] B. Timmermans, N. Vaeck, A. Hubin, and F. Reniers, Chemical effects in Auger electron spectra of aluminium, *Surface and Interface Analysis* **34**, 356 (2002).
- [24] G. E. McGuire, *Auger Electron Spectroscopy Reference Manual* (Springer US, 1979).
- [25] We note that the largest feature in these measured spectra can be found at 1404 eV, while the largest feature in the elemental aluminum reference spectrum in [24] is located at 1389 eV. We attribute this mismatch to electron-analyzer calibration differences.
- [26] C. G. Pantano and T. E. Madey, Electron beam damage in Auger electron spectroscopy, *Applications of Surface Science* **7**, 115 (1981).
- [27] M. E. Drits, E. S. Kadaner, and L. S. Toropova, Recrystallization of aluminum and aluminum alloy foils, *Metal Science and Heat Treatment* **13**, 399 (1971).
- [28] G. E. Rhead, Atomic mobility at solid surfaces, *International Materials Reviews* **34**, 261 (1989).
- [29] C. V. Thompson, *Annu. Rev. Mater. Sci.*, Tech. Rep. (1990).
- [30] U. Valbusa, C. Boragno, and F. Buatier de Mongeot, Nanostructuring by ion beam, *Materials Science and Engineering C* **23**, 201 (2003).
- [31] S. Rusponi, G. Costantini, C. Boragno, and U. Valbusa, Scaling laws of the ripple morphology on Cu(110), *Physical Review Letters* **81**, 4184 (1998).
- [32] Y. Yamamura and H. Tawara, Energy dependence of ion-induced sputtering yields from monatomic solids at normal incidence, *Atomic Data and Nuclear Data Tables* **62**, 149 (1996).
- [33] S. Ri and M. Saka, Diffusion-fatigue interaction effect on hillock formation in aluminum thin films under thermal cycle testing, *Materials Letters* **79**, 139 (2012).
- [34] P. Dutta and P. M. Horn, Low-frequency fluctuations in solids: 1/f noise, *Reviews of Modern Physics* **53**, 497 (1981).
- [35] M. B. Weissman, 1/f noise and other slow, nonexponential kinetics in condensed matter, *Reviews of Modern Physics* **60**, 537 (1988).
- [36] G. P. Zhigalskii, Zhigalskii1997 - 1f noise and nonlinear effects in thin metal films, *Physics - Uspekhi* **40**, 559 (1997).
- [37] J. W. Eberhard and P. M. Horn, Excess (1f) noise in metals, *Physical Review B* **18**, 6681 (1978).
- [38] K. Y. Lin, G. H. Low, and I. L. Chuang, Effects of electrode surface roughness on motional heating of trapped ions, *Physical Review A* **94**, 013418 (2016).
- [39] R. Dubessy, T. Coudreau, and L. Guidoni, Electric field noise above surfaces: A model for heating-rate scaling law in ion traps, *Physical Review A* **80**, 031402(R) (2009).
- [40] G. H. Low, P. F. Herskind, and I. L. Chuang, Finite-geometry models of electric field noise from patch potentials in ion traps, *Physical Review A* **84**, 053425 (2011).
- [41] S. S. Yeh, W. Y. Chang, and J. J. Lin, Probing nanocrystalline grain dynamics in nanodevices, *Science Advances* **3**, e1700135 (2017).
- [42] M. Berlin-Udi, *Treatments of a Surface Ion Trap: A Study of Electric-Field Noise near a Contaminated Metal Surface*, Ph.D. thesis, University of California, Berkeley (2020).
- [43] P. Dutta, P. Dimon, and P. M. Horn, Energy Scales for Noise Processes in Metals, *Physical Review Letters* **43**, 646 (1979).
- [44] J. Briggmann, K. Dagge, W. Frank, A. Seeger, H. Stoll, and A. H. Verbruggen, Irradiation-induced defects in thin aluminium films studied by 1/f noise, *physica status solidi (a)* **146**, 325 (1994).
- [45] R. H. Koch, J. R. Lloyd, and J. Cronin, 1/f noise and grain-boundary diffusion in aluminum and aluminum alloys, *Physical Review Letters* **55**, 2487 (1985).
- [46] J. V. Barth, *Surface Science Reports*, Tech. Rep. 3 (2000).